Immersion Lithography: Photomask and Wafer-Level Materials

Roger H. French and Hoang V. Tran

DuPont Co. Central Research, E400-5207 Experimental Station, Wilmington, DE 19880-0400; email: roger.h.french@usa.dupont.com

Annu. Rev. Mater. Res. 2009. 39:93–126

First published online as a Review in Advance on March 3, 2009

The *Annual Review of Materials Research* is online at matsci.annualreviews.org

This article's doi: 10.1146/annurev-matsci-082908-145350

1531-7331/09/0804-0093$20.00

Key Words

photoresist, pellicle, high-index fluid, phase shift, double patterning

Abstract

Optical immersion lithography utilizes liquids with refractive indices >1 (the index of air) below the last lens element to enhance numerical aperture and resolution, enabling sub-40-nm feature patterning. This shift from conventional dry optical lithography introduces numerous challenges requiring innovations in materials at all imaging stack levels. In this article, we highlight the recent materials advances in photomasks, immersion fluids, topcoats, and photoresists. Some of the challenges encountered include the fluids' and photomask materials' UV durability, the high-index liquids' compatibility with topcoats and photoresists, and overall immersion imaging and defectivity performance. In addition, we include a section on novel materials and methods for double-patterning lithography—a technique that may further extend immersion technology by effectively doubling a less dense pattern's line density.

1. INTRODUCTION

Photoresist: light-sensitive polymer formulations used to define structural features in integrated-circuit processing

Deep UV light (DUV): normally referring to the 248-nm peak intensity of the KrF excimer laser

In semiconductor fabrication optical lithography, the main materials development has traditionally been polymeric photoresists, which changed substantially each time the lithographic wavelength decreased: from 436 nm (G-line) to 365 nm (I-line) to 248 nm [deep UV light (DUV)] to the current 193 nm. For example, the shift to DUV (KrF excimer laser) coincided with the introduction of chemically amplified resists. Currently, the transition to 193 nm (ArF excimer laser), along with a failed transition to 157 nm (F_2 excimer laser), has expanded greatly the number and type of materials needed above and below the projection lens in lithographic scanners (**Figure 1**). These new materials include both photomask materials (**Figure 2**) as well as new types of wafer-level materials, such as immersion fluids (**Figure 3**). These new materials—photomasks, pellicles,

Figure 1

ASML TwinScan XT:1950i scanner showing the illuminator, the reticle (photomask) and reticle handler, the projection lens, and the wafer stages. The illuminator, which prepares the ArF excimer laser light, is on the right. The photomask on the left side, above the large cylindrical projection lens, and the dual-wafer stages below the projection lens are shown, with the left wafer stage undergoing alignment procedures. Meanwhile, the right wafer stage, under the last lens element of the projection lens, is exposing the fields of the wafer under water immersion conditions. The numerical aperture of this water immersion stepper is 1.35, and the productivity is >140 wafers per hour imaged. Image reprinted courtesy of ASML Inc., Veldhoven, The Netherlands.

Figure 2

Two photomasks with pellicles. The upper mask is a conventional binary-intensity mask, with the mask pattern and the pellicle on the lower surface of the 6 × 6 inch ultrahigh-purity fused silica photomask substrate. The lower mask is a negative-tone phase shift mask, and the mask pattern and the pellicle are on the upper surface of the substrate. Photograph reprinted courtesy of Toppan Photomasks Inc., Round Rock, Texas.

photoresists, bottom antireflection coatings (BARCs), and topcoats—coupled with the introduction of immersion lithography, have enabled much larger optical scanner numerical aperture (NA) lenses (up to 1.35 NA with water as the immersion fluid), enabling 45-nm half-pitch feature printing using 193-nm light. Before the 1993 lithographic materials review published in this journal's predecessor (1), the focus was on photoresists and advances in chemically amplified resists. Today, immersion lithography's development has led to the introduction of immersion fluids, topcoats, and novel photoresist components to manage fluid-resist interactions and to reduce any possible lens contamination. Immersion lithography materials have become a broad, diverse, and complex family developed to help the industry's advance to 32-nm half-pitch feature sizes. At the same

Scanner (or stepper): the processing tool used in the main lithographic imaging step in advanced integrated-circuit processing

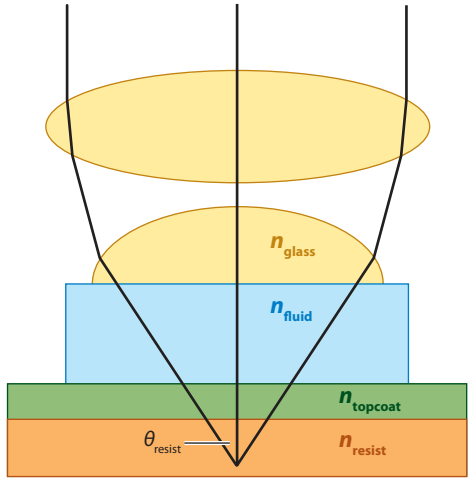

Figure 3

Immersion lithography imaging stack showing the projection lens optics, including the last lens element contacting the immersion fluid, and a topcoat layer on top of the photoresist layer. Adapted from Reference 34, with permission from SPIE.

Photomask: lithographic photomasks are typically transparent fused silica blanks covered with a pattern defined with a chrome metal absorbing film

Pellicle: a thin transparent film stretched over a frame that is glued over one side of the photomask to serve as a dust protector

Bottom antireflection coating (BARC): an inorganic or organic thin film used between the photoresist and the semiconductor wafer, used to control the reflectance of light from the wafer back up into the photoresist layer

Topcoat: a polymer coating used above the photoresist to reduce interactions between a photoresist and an immersion fluid

time, the possible uses of second-generation immersion fluids, double or triple patterning, and novel resist processes indicate that the need for new and optimized materials will not be reduced in the future.

1.1. Microfabrication

Microfabrication—first developed for integrated circuit processing—has relied on photolithography as a critical pattern transfer process. From the first transistor in 1947 and the first integrated circuit (IC) or semiconductor device in 1959, the basic microfabrication process steps have been deposition, etch, implant, and patterning (2). Patterning has included photolithography in either contact or proximity modes (where the photomask and the IC have the same 1:1 feature size ratio) as well as the now dominant projection mode (where there is a 4:1 or 5:1 optical reduction of the mask features to the IC feature sizes). Rayleigh's equations (3) provide a simple relationship between the stepper/scanner optical parameters—such as the lithographic wavelength (λ), the lens numerical aperture [NA = sin(θ) where θ is the half cone angle of focus], the imaging medium's refractive index (1 for air and higher for immersion fluids)—and the feature size (FS) and depth of focus (DOF) that can be achieved. These equations also include a process latitude factor (k), where k_1 corresponds to the FS equation (Equation 1) and k_2 the DOF equation (Equation 2), and where we define the scanner's NA as $NA_{System} = NA_{Dry}\, n_{Imaging\,medium}$, where n is the index of refraction of the immersion fluid determined at the lithographic wavelength λ (4). k depends on the overall process capability, and thereby includes the beneficial imaging contributions of phase shift masks, photoresists with improved imaging, and development characteristics along with stepper settings, such as dipole or quadrapole illuminations, which are beyond the simple NA and λ characteristics of the scanner. Microfabrication's progression down this Moore's law (5–7) feature size path for complementary metal oxide semiconductor (CMOS) devices has been enabled by technological advances in optics, usable lithographic wavelengths, and most recently, immersion fluids to allow projection lens NAs above 1. We summarize this lithography evolution in **Table 1**, where we include half pitch feature sizes and the corresponding Rayleigh's equation parameters,

with the associated lithography tool characteristics and lithography materials choices. This can serve as a roadmap to the materials science discussed in this review. During this lithography evolution, microfabrication and optical lithography have also expanded beyond semiconductor ICs to include flat-panel displays, microelectronic machines and devices, photovoltaic solar cells, and other applications, further driving the motivation to improve optical lithography's capabilities. In addition, as IC feature sizes have decreased, physical limits on materials and processes have led to new materials and device architectures, such as the IC interconnect conversion from aluminum to dual damascene copper metallization, the transition from silica interconnect dielectrics and gate dielectrics, and new gate architectures [such as the strained gate or 3-D gate geometries of FinFET devices (8)]. Both microfabrication's widening applications and the incorporation of new materials, process technologies, and architectures into IC fabrication demonstrate the broad platform that microfabrication represents for materials research, as well as the large technology base it provides to the semiconductor, display, and photovoltaic industries.

$$\mathrm{FS} = k_1 \lambda / \mathrm{NA}, \quad 1.$$

$$\mathrm{DOF} \approx k_2 \lambda / \mathrm{NA}^2, \quad 2.$$

1.2. Nanofabrication and Soft Lithography

During photolithographic patterning's ongoing development for microfabrication, there have been parallel efforts on novel new technologies to displace photolithography. For example, X-ray proximity lithography, ion beam and e-beam projection, and e-beam direct-write lithography have all been the focus of large and substantial research and development efforts. However, other than the critical role that e-beam direct-write has played in photomask patterning for optical lithography, none of these technologies has succeeded in displacing optical projection lithography (9). E-beam direct-write has been pursued in both single e-beam and massively parallel multibeam modes—the latter to improve the technology's pattern transfer rate and to compete with projection optical lithography's productivity. Instead of hard X-ray proximity lithography, there has been substantial research in the past 15 years on soft X-ray projection lithography [now called extreme UV (EUV) lithography] using 13.5-nm light and multilayer reflective mirror optics; this technology is now considered a next-generation lithography to replace optical projection lithography. For more on EUV lithography materials issues, see the article in this volume by Sewell & Mulkens (10).

There has been much recent work on soft lithography: imprint lithography whereby either stamping with an elastomeric patterned mask, or hard mask contacting either photo or thermally polymerizable materials, allows direct pattern transfer (11). This nanoimprint technology, discussed in an article in this volume by Willson and coauthors (12), can make very fine feature sizes. There is also recent work on dip pen lithography, or scanning probe lithography, which (like e-beam direct write) utilizes an atomic force microscope tip to directly write the pattern either with a single probe or with a probe array (13). In addition, there is much research on both self-assembly of small molecules and oligomers, as well as templated growth. Templated growth involves the exploitation of small structural features (which may be introduced by patterning) to construct complex functional materials or devices that use materials growth on the template. Ross provides an example in discussing patterned magnetic media (14).

1.3. The Ongoing Evolution of Photolithography

Projection optical lithography (or photolithography) has continued meeting semiconductor device makers' patterning needs since the industry's inception, with photolithographic advances

Integrated circuit (IC): also referred to informally as a computer chip

Depth of focus (DOF): a defining parameter in a photoresist's imaging performance; the depth range of the wafer over which the feature sizes are within specification. Typically defined as the wafer plane height variation that leads to a +/−10% variation of the critical dimension (CD), or width, of the lithographically printed feature

Moore's law: an empirical relationship first stated by Intel cofounder Gordon Moore in 1965, i.e., the number of transistors in an integrated circuit doubles (at approximately constant cost) every two years

Extreme UV light (EUV): the plasma-generated 13.5-nm radiation being studied for advanced integrated-circuit photolithographic applications

Table 1 Lithography evolution over the years, from I-line to EUV, as semiconductor half pitch feature sizes have evolved from 400 nm to 22 nm

Hp (nm)	400	300	250	180	130	90	90	90	90	65	65
Technology	365 Dry	365 Dry	248 Dry	248 Dry	248 Dry	248 Dry	193 Dry	193 Dry	157 Dry	157 Dry	193 Dry
Commercialized as of 2009?	Yes	Yes	Yes	Yes	Yes	Yes	Yes	Yes	No	No	Yes
λ (nm)	365	365	248	248	248	248	193.4	193.4	157.6	157.6	193.4
Index	1	1	1	1	1	1	1	1	1	1	1
NA	0.6	0.65	0.63	0.8	0.8	0.93	0.75	0.85	0.75	0.85	0.93
k1	0.66	0.53	0.64	0.58	0.42	0.34	0.35	0.40	0.43	0.35	0.31
Light source	Hg lamp	Hg lamp	KrF laser	KrF laser	KrF laser	KrF laser	KrF laser	ArF laser	F2 laser	F2 laser	ArF laser
Lens material	Glass	Glass	SiO_2	SiO_2	SiO_2	SiO_2	SiO_2	SiO_2	CaF2	CaF2	SiO_2
Pellicle	Nitro-cellulose	Nitro-cellulose	Fluoro-polymer	Fluoro-polymer	Fluoro-polymer	Fluoro-polymer	Fluoro-polymer	Fluoro-polymer	Fluoro-polymer	Fluoro-polymer	Fluoro-polymer
Photomask	Binary Intensity Mask	Binary Intensity Mask	Binary Intensity Mask	Binary Intensity Mask	Attenuated PSM	PSM	PSM	Attenuated PSM	Binary Intenstiy Mask	PSM	PSM
Fluid	None	None	None	None	None	None	None	None	None	None	None
Topcoat	None	None	None	None	None	None	None	None	None	None	None
Photoresist	Novolak	Novolak	Styrenic systems	Styrenic systems	Styrenic systems	Styrenic systems	Methacrylic systems	Methacrylic systems	Fluoro-polymer	Fluoro-polymer	Methacrylic systems

This table includes lithographies that were successfully commercialized and others that failed in development, while still advancing the science of lithographic materials. We also include information of the different materials that have been chosen for different aspects of the lithography, such as pellicles, photomasks, immersion fluids, topcoats, and photoresists.

providing a large part of the feature size/density improvements that contribute to Moore's law advances (15). The main drivers of these advances have been the shifts to shorter lithography wavelengths, improvements in stepper or scanner illuminators and projection lens optics, and photoresist improvements. The movement over the years to shorter lithography wavelengths has progressed from the mercury emission lines of G-line (436 nm) all the way to 193 nm (ArF excimer) and most recently and unsuccessfully, 157 nm (F_2 excimer). In 1976, G-line light was used with contact or proximity lithography (with a mask aligner still found to this day) and diazonaphthoquinone/novolak resists to produce 5–6-μm feature sizes (16). By 1987, the state of the art had approached 1-μm feature sizes using I-line wavelengths, as well as projection lithography with a 4× reduction between the mask and the pattern produced in the photoresist (17). The next step was to enter the submicrometer lithography regime, which was considered a great optical projection lithography challenge and was not certain to be achieved. Submicrometer lithography was enabled by introducing 248 nm as the lithographic wavelength—initially from mercury lines and then from KrF excimer lasers—coupled with the development of chemically amplified photoresists based on polyhydroxystyrene (PHOST). In these photoresists, a photoacid generator (PAG) (excited by the 248-nm light) would photocatalytically decompose the positive photoresist, leading to a large number of deprotection events from a single absorbed photon. This advance dramatically improved 248-nm lithography's sensitivity and also led to unprecedented photolithographic pattern formation control such that by 1993 feature sizes of 0.5 μm were produced in commercial ICs. Subwavelength lithography was enabled not only by improved photoresist processes, but also by the introduction of phase shift photomasks, which took advantage of phase of the light: Instead of intensity based on photoresist exposure [as with a traditional

Photoacid generator (PAG): a photoresist formulation component that generates a proton on exposure to light at the lithographic wavelength

Table 1 (*Continued*)

65	55	45	38	38	32	32	32	32	28	22	22
193 H_2O SP	193 H_2O SP	193 H_2O SP	193 H_2O SP	193 Gen2 SP	193 Gen2 SP	193 Dry DP	193 H_2O DP	EUV	193 Gen3 SP	193 H_2O DP	EUV
Yes	Yes	Yes	Yes	No	No	No	Yes	No	No	No	No
193.4	193.4	193.4	193.4	193.4	193.4	193.4	193.4	13.5	193.4	193.4	13.5
1.44	1.44	1.44	1.44	1.64	1.64	1	1.44	1	1.9	1.44	1
0.93	1.2	1.35	1.35	1.55	1.55	0.85	1.35	0.25	1.8	1.35	0.32
0.31	0.34	0.31	0.27	0.30	0.26	0.14	0.22	0.59	0.26	0.15	0.52
ArF laser	ArF laser	ArF laser	ArF laser	ArF laser	ArF laser	ArF laser	ArF laser	EUV LPLS	ArF laser	ArF laser	EUV LPLS
SiO_2	SiO_2	SiO_2	SiO_2	SiO_2 & LuAG	SiO_2 & LuAG	SiO_2	SiO_2	None-Reflective Mirrors	SiO_2 & LuAG	SiO_2	None-reflective mirrors
Fluoro-polymer	Fluoro-polymer	Fluoro-polymer	Fluoro-polymer	Fluoro-polymer	Fluoro-polymer	Fluoro-polymer	Fluoro-polymer	None	Fluoro-polymer	Fluoro-polymer	None
PSM	PSM	PSM	PSM	PSM	PSM	PSM	PSM	Binary Intensity Reflective Mask	PSM	PSM	Binary Intensity Reflective Mask
Water	Water	Water	Water	Hydrocarbons	Hydrocarbons	None	Water	None	Unknown	Water	None
Fluorinated	Fluorinated	Fluorinated	Fluorinated	Unknown	Unknown	None/CEL	Fluorinated	None	Unknown	Fluorinated	None
Methacrylic systems	Methacrylic systems	Methacrylic systems	Methacrylic systems	Methacrylic systems	Methacrylic systems	Spacer/ freezing systems	Methacrylic systems	Styrenic systems	HI resists	Methacrylic systems	Styrenic systems

binary-intensity mask (BIM)], adding phase contrast to the latent image formation enhances the ability to produce subwavelength features. Attenuating phase shift masks (APSMs) are discussed below; for I-line lithography, they enabled 250-nm feature printing using 365-nm light in 1994.

Since the last *Annual Review of Materials Research* (and predecessor journal) articles on lithography (1, 16–18), there have been advances in our quantitative understanding of the physics and chemistry of photoresist imaging and etching, giving new insights into the polymer interfaces (18) that result from photolithography. For example, the study of both line edge roughness (LER) or line width roughness (19) has become critical; LER can now account for a major portion of line width variation. The line roughness fundamentals obtained from the imaging process' photochemistry have been extensively examined by new experimental methods characterizing the reaction-diffusion front (20) in chemically amplified resists using infrared spectroscopy (21) and X-ray absorption fine structure (22). These new approaches have also played an important role in immersion lithography by elucidating the role of the size of the PAGs in imaging (23). In addition, the photoresists' robustness under etch conditions and the resulting surface roughness levels have become a focus of study (24). These experimental advances have also been coupled with a more detailed understanding of the photoimaging process, resulting in improved quantitative metrics for comparing photoresists' performance (25).

It appears that 193-nm photolithography could be the last optical lithography generation, extended by immersion lithography versus making another wavelength change (26). Research on 193-nm optical lithography began in the early 1990s and immediately had challenges: PHOST resists were too optically absorbing to 193-nm light; moreover, SiO_2 glass exhibited densification under 193-nm irradiation, producing damaging aberrations in the projection optics.

These problems were addressed by new photoresist compositions, with the methacrylate resists being most commonly used today for 193-nm resists, and by tighter control of the glass composition and stoichiometry, thus removing the densification-induced optical aberrations. With these improvements, 193-nm lithography was introduced in commercial production in the early 2000s and is now the dominant photolithography for leading-edge production.

Once the research and development pipeline for 193-nm lithography was under way, 157 nm from F_2 excimer lasers was proposed in 1997 as the next lithography wavelength, with research and development starting in earnest in 1999 (27). For 157-nm lithography, the number of challenges was even larger: SiO_2 glass, photoresist polymers, and pellicle polymers are not transparent at 157 nm (pellicles are used as in situ dust covers on photomask reticles). Therefore, a suite of new materials, with CaF_2 the designated lens material and fluorine-doped SiO_2 the glass for photomask substrates, and much work were needed to develop photoresist and pellicle polymers. Considerable progress in materials research was achieved on 157-nm photolithography. However, in the end, 157-nm lithography failed in 2003 owing to an inability to produce CaF_2 of the required optical quality (acceptable levels of stray light and flare arising from scattering in the material) for a projection lens.

In 2002, immersion lithography (28) was proposed. For the first time in optical lithography's history, the transition was not from wavelength to wavelength. Instead, the transition involved changing the imaging medium between the lens and the photoresist-coated wafer, from air (193-nm refractive index = 1) to a liquid such as water (193-nm refractive index = 1.436). With the imaging being done under water, the effective wavelength of a 193-nm ArF excimer laser is reduced to 193.4/1.436 = 134.7 nm. Thus, the imaging wavelength in essence shrinks while still using an established light source. This advance avoids extensive CaF_2 crystal use for the projection lens because the reduction lens remains in air, and only below the last lens element is imaging done in the immersion fluid. The optical lithography roadmap now appears to have its terminal lithography wavelength, 193.4 nm (29, 30).

1.4. Development and Performance of Immersion Imaging

Immersion lithography has led to radical changes in optical scanner design such that the immersion fluid can be contained between the projection lens' last element and the photoresist-coated silicon wafer while still allowing a high process throughput (greater than 120 wafers h^{-1}). The scanner manufacturers [ASML (31), Nikon (32, 33), and Canon] have all chosen water as the first-generation immersion fluid and have evaluated many different approaches to immersion lithography's technical challenges. For example, different immersion fluid containment methods were considered; such methods included a fluid bath in which the wafer would reside, a showerhead in which the fluid would continuously flow from the showerhead onto the wafer, and be removed from the wafer by the showerhead assembly, and another approach in which the fluid would be deposited on the wafer by a showerhead but would flow over the wafer edges to a drain. The final solution seems to be the showerhead, or immersion hood, in which the fluid is deposited and removed by the showerhead, and the fluid is flowing continuously, with the water temperature maintained to very high precision to minimize any imaging artifacts arising from water's refractive index change with temperature (i.e., dn/dT). Another critical aspect, necessary to control the number of immersion-specific defects per wafer, is to carefully control the showerhead movement over the wafer's edge. Another important consideration centers on the track: the wafer processing system directly attached to the photolithographic scanner, which is used to coat the imaging stack [consisting of a bottom antireflection coating (BARC), the photoresist layer, and sometimes a topcoat] and to perform any necessary postapplication thermal bake steps. The track then supplies

the wafers into the scanner at a rate of more than 120 wafers h^{-1} and receives the exposed wafers back for postexposure bake, development in tetramethylammonium hydroxide (TMAH), and spin drying. Typically, photoresist is removed from a small rim around the wafer's edge, using an edge bead remover in the original photoresist coating process, because the wafer's high speed and fast acceleration relative to the stationary showerhead can lead to particulate delamination from the wafers edge, generating immersion defects on the final imaged wafer.

Ongoing immersion lithography materials research and development have included developing next-generation immersion fluids (34) [building on earlier work on immersion fluids for use in 157-nm lithography (35)] that have higher refractive indices so as to replace water immersion fluids and thus further increase the scanner's NA.

Tetramethylammonium hydroxide (TMAH): in the integrated-circuit industry, the 0.26 molar aqueous solution normally used to develop the light-exposed photoresist

1.5. The Next Generation of Lithography?

The next-generation lithography, if successfully brought into commercial-scale IC fabrication, appears to be either EUV lithography, imprint lithography, or massively parallel e-beam direct write (36). But it is certain that 193-nm lithography will be extended as far, and for as long, as it is commercially viable. This ongoing extension will make use of as many optical enhancements (phase shift, polarization) and variations such as double (and perhaps triple) patterning, thus providing an ongoing set of research and development challenges for materials scientists.

2. PHOTOMASK MATERIALS

With the advent of subwavelength lithography, the imaging properties of the photomask (i.e., the object in the scanner that is imaged into the photoresist) (37, 38) have attained critical importance, such that full 3-D imaging codes are used, and the opaque chrome film used in BIMs has changed to become both thinner and more opaque. In addition, the introduction of resolution enhancement techniques (130) such as phase shift masks and optical proximity corrections (39, 40) has broken the simple and long-standing idea that the mask (object) is a replica of the desired circuit layout (image). Instead, one must now consider the full scanner imaging, including the properties of both the object and the image stack. This results in a complex optimization that is tied to the desired circuit pattern (such as contact layer, gate, interconnect), the particular scanner used, the particular photomask and type (BIM, APSM, alternating PSM, etc.), and wafer-level imaging stack (41, 42). Lithography has now become computationally intensive, with iterative refinements needed to achieve accurate fidelity and yield in the fab. These requirements lead to detailed thin-film optimization for both binary (43, 44) and phase shift (45, 46) masks, consideration of the effects of the pellicle and mask flatness (48) on the lithographic imaging, and optical proximity corrections (47) of the lines in the circuit layout to print the desired features. In the 1970s and 1980s, before these advances, imaging was considered simple. Now, mask and wafer-level materials development must be closely coupled to lithographic image modeling to achieve the desired effects while minimizing undesirable artifacts.

2.1. Attenuating Phase Shift Photomasks

APSMs have been widely accepted in lithography for providing phase contrast imaging without the extra process steps (e.g., trim masks) needed for strong phase-shifting approaches such as alternating phase shift masks. We have developed APSMs for I-line, DUV, and 193-nm lithography. The I-line masks met with commercial acceptance, while thin films based on molybdenum and silicon (MoSi) (49) have become the dominant materials used at DUV and 193-nm wavelengths.

In these photomasks, the thin film attenuates the light to 6% or 9% (50) of the mask's illuminating intensity and also phase shifts this light by 180° relative to the light transmitted through the openings (the mask's lines) in the thin film. This attenuated phase-shifted light then destructively interferes with the light transmitted by the lines, thereby reducing the lithographically printed line width.

2.1.1. I-line attenuated phase shifters. When lithography first went subwavelength, many different phase shift approaches were studied, but the ease with which APSMs could be incorporated made them especially attractive. Traditional opaque BIMs are made from films of Cr-OCN prepared by reactive sputter deposition, producing a compositionally graded film that is optically shiny when viewed through the fused silica substrate but that is light brown when viewed from the film side. The light brown side serves as an antireflection coating, reducing stray light on the projection lens side of the mask. For use at I-line, the required 6–9% transmission with 180° of phase shift was produced by adjusting Cr-OCN composition and gradient while simultaneously maintaining the Cr-OCN film's critical wet etch properties for the transfer of the e-beam written mask layout into the chrome film (51). This process involves both changing the properties and relative amounts of CrN (metallic) compounds and CrO (antireflection) compounds and also adjusting the level of C present throughout the film for etch properties (as shown in **Figure 4** for a 6% transmission I-line attenuated phase shift film). Understanding these optically inhomogeneous films required developing novel ellipsometric modeling methods to determine the films' graded optical properties (52). These I-line APSMs (53) were among the first phase-shifting masks used in commercial production. Their acceptance was based on three critical factors: the industry familiarity with chrome; the ability to do research and development on commercial production equipment, reducing the process transfer hurdle from research (54); and the economic drivers that enabled customers to print 250-nm features with 365-nm light, thus delaying investments in DUV equipment and processes. The compositional family of the Cr-OCN compounds was also studied to define a rich set of process/property relationships (55).

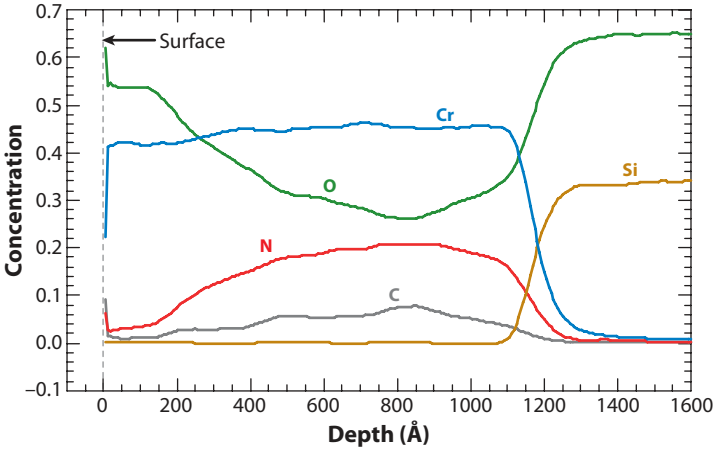

Figure 4

Composition profiles from sputtered neutrals mass spectroscopy showing composition gradients in a CrOCN thin film used as an I-line attenuating phase shift photomask. Composition is given on an absolute basis, which sums to 1.0. Adapted from Reference 55.

2.1.2. Deep UV light and 193-nm attenuated phase shifters. APSMs for 248-nm and 193-nm lithography could not be fabricated using Cr-OCN films owing to Cr's high optical absorbance. Therefore, a materials screening study was undertaken (56), determining what two component materials to use in what type of microstructure to produce the tunable optical material needed. Other researchers settled on compositionally graded films of MoSi (more accurately, compounds of Mo and Si with O, N, and C). We developed multilayer films of AlN with TiN (optical superlattices) produced by sequential multilayer ion beam deposition, in which the bilayer thickness was kept to less than $\lambda/20$ (i.e., less than 10 nm). These films were thus optically homogeneous and behaved optically as uniform films, even though the AlN and TiN amounts in each bilayer were the variables used to produce optical tunability (57). This material family produced APSMs with transmissions from 6% to 20% with a 180° phase shift for both 248 and 193 nm (58). We also developed another APSM family consisting of organic/inorganic hybrids of Teflon® AF with organosiloxane compounds. In this case, the organosiloxane phase was used to tune the optical constants as needed for the phase shifter design (59). These technologies were developed and evaluated by the industry but did not reach commercialization. Materials design of new APSMs continues as an active research field, as demonstrated by the research of Lai and colleagues (60, 61).

2.2. Polymers for Photomask Pellicles

Pellicles are thin polymer membranes supported on aluminum frames and mounted on a photomask's patterned film side—typically 6 mm above the masking film (**Figure 2**). They assure that any dust particles falling onto the photomask are out of the object plane of the objective lens and therefore are not present in the image formed in the photoresist layer by the photomask.

2.2.1. Cytop and Teflon AF. In G-line or I-line lithography, the pellicle membranes are initially fabricated from high-molecular-weight nitrocellulose polymers; the membrane is prepared by spin coating from a polymer solution onto a glass plate. The aluminum frame is then adhesively attached to the polymer membrane, followed by membrane release from the glass plate, trimming of the membrane edges at the frame, and optical inspection of the pellicle for any defects. The pellicle thickness is chosen so that the membrane's interference fringes give a maximum transmission. With the advent of DUV lithography, nitrocellulose was no longer sufficiently transparent, so amorphous fluoropolymers such as Teflon AF (62) or Cytop (from Asahi Glass Company, Tokyo), which have optical absorption edges at much shorter wavelength (**Figure 5**), were developed. The thickness of the pellicle membrane can be optimized to give its peak interference transmissions at multiple wavelengths; for example, a thickness on the order of 0.8 μm can be used for I-line and DUV lithography.

2.2.2. Novel fluoropolymers. As can be seen in **Figure 5**, the commercial amorphous fluoropolymers have appreciable absorbance at 157 nm. Films of Teflon AF 1600 and Cytop™ that are 1 μm thick have 157-nm transparency of no more than 38% and 2%, respectively, making them unsuitable for use as 157-nm pellicle materials. At the same time, a pellicle's use is an essential requirement to enable defect free lithographic printing in a production environment. For example, EUV lithography is being pursued as a next-generation lithography, and the lack of EUV pellicle technology is a major challenge. For 157-nm lithography, researchers developed fluoropolymers (63) that had optical absorption edges at much shorter wavelengths than did Teflon AF 1600 or Cytop (**Figure 6**). Polymers such as $-[(CH_2CHF)_xC(CF_3)_2CH_2]_y-$ or $-(CH_2CF_2)_x$[2,2-bis(trifluoromethyl)-4,5-difluoro-1,3-dioxole]$_y-$, with chains that alternate fluorocarbon segments with either oxygen or hydrocarbon segments, frequently show >98% transparency at 157 nm

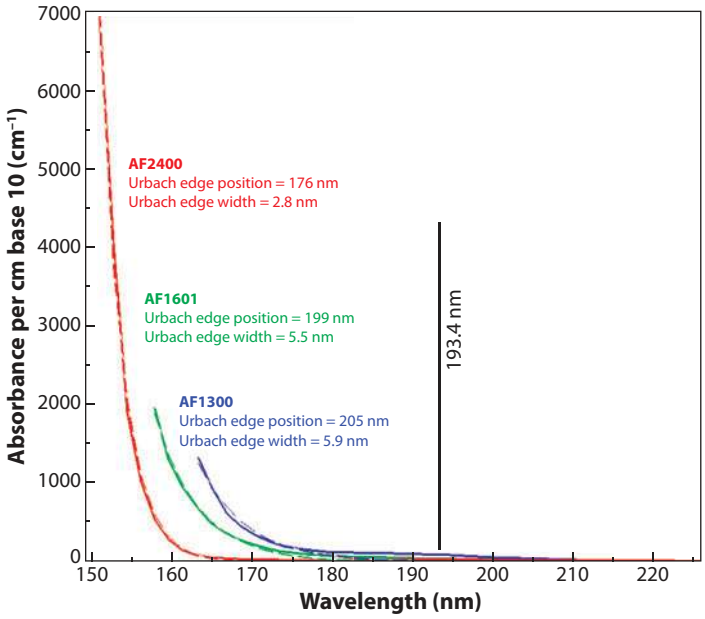

Figure 5

Optical absorption edge [fits to the optical absorbance-cm^{-1} (base 10)] of three grades of Teflon® AF with their corresponding Urbach edge fits (*dashed lines*) showing the absorption edge position and width. Solid lines denote measured data. Adapted from Reference 62, with permission from SPIE.

(if these polymers are amorphous). These polymers are made from monomers such as vinylidene fluoride (VF_2) and hexafluoroisobutylene, which themselves exhibit good structural alternation of CH_2 and CF_2. In addition, ether linkages can force alternation, and fluorocarbon segments shorter than six carbons and hydrocarbon segments shorter than two carbons (or shorter than three carbons if the segments are partially fluorinated), also promote 157-nm transparency. Even with these design principles, it is advantageous to avoid small rings such as cyclobutanes. These results suggest a steric component to transparency besides the importance of alternation.

Pellicles must have long lifetimes under lithographic wavelength irradiation, given the time and expense of repellicalization: sub–class 1 clean room, patterned mask cleaning, and new pellicle frame attachment. These steps may introduce new defects or even damage the patterned film. Therefore, a typical pellicle lifetime requirement corresponds to a 7.5 kJ cm^{-2} dose at the lithographic wavelength. Compared with Teflon AF 1600 and Cytop, which exhibit a pellicle lifetime at 157 nm that is measured in millijoules, the novel fluoropolymers developed for use as 157-nm pellicles had lifetimes below 10 J cm^{-2}.

Upon irradiation, these polymers undergo photochemical darkening, with none demonstrating the kilojoule radiation durability lifetimes required for commercial viability. These lifetimes are likely because the requirements are such that every bond absorbs >10 photons, each having an energy roughly twice common bond energies. We (64) have studied intrinsic (composition, molecular weight) and extrinsic (trace metals, impurities, environmental contaminants, oxygen, water) contributions to optical absorption and photochemical darkening in these polymers. Studies in model molecules illustrate the dynamics of photochemical darkening and show that appreciable lifetimes can be achieved in fluorocarbons. To a first approximation, the polymers that have lower 157-nm optical absorbance also tend to show the longest lifetimes. These results imply that quantum yield, or the extent to which the polymer structure can harmlessly dissipate energy, can

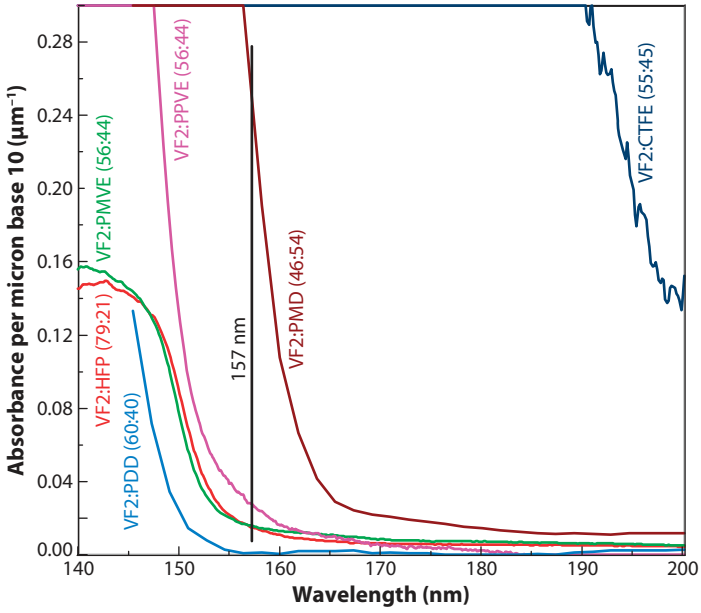

Figure 6

Absorption edges of experimental TAFx fluoropolymers. Optical absorption edge of vinylidene fluoride copolymers, with their monomer ratios in parentheses, showing low absorbance at 157 nm. The optical absorbance spectra [in units of 1 per micrometer (base 10) versus wavelength] show the effects of transmission measurement saturation, as evidenced by a plateau at higher absorbance values and shorter wavelengths (owing to the low transmission of the samples at these wavelengths). This figure, and information on more copolymers, can be found in Reference 63, with permission from Elsevier.

be important as well (65). In parallel with developing polymeric pellicles, fused silica glass pellicles were developed and showed promising optical performance.

3. MATERIALS IN THE LITHOGRAPHIC IMAGING STACK

The immersion lithography materials required on the image side (i.e., below the projection lens) also span a wide variety of materials and classes. These materials include the immersion fluids, topcoats (used to separate the fluid from the imaging photoresist film), the photoresist layer, and an antireflection layer underneath. We discuss these in order below.

3.1. Immersion Fluids

Immersion fluids yield enhanced imaging performance in the same way that water or oil immersion techniques improve an optical microscope's resolution. When imaging is performed in a fluid that has a refractive index of >1 (1 is the value for air), the light's wavelength is effectively reduced by the fluid's index. The fluids must be optically transparent (i.e., have a low optical absorbance at the lithography wavelength) and must have a high refractive index. The first immersion fluids studied were to be used to extend 157-nm lithography, but it is immersion lithography at 193 nm using water that has been successfully commercialized.

Water-based immersion lithography using 193-nm ArF illumination provides optical solutions as far as the 45-nm node (with a k_1 of 0.31) but is not able to achieve the 38-nm or 32-nm

nodes as currently defined. Achieving these lithographic nodes will require new, higher-refractive-index fluids to replace the water used in first-generation immersion systems. Therefore, there has been extensive research to develop second-generation ($1.44 \leq n_{193\,nm} \leq 1.65$) and third-generation ($1.65 \leq n_{193\,nm} \leq 1.8$) 193-nm immersion fluids. We have developed a number of such second-generation high-index fluids for immersion lithography at 193 nm, with low optical absorbance and refractive indices up to 1.664. To understand different fluid classes' behavior and performance, we use spectral index measurements to characterize the index dispersion, coupled with Urbach (66) absorption edge analysis and Lorentz oscillator modeling (34).

Compared with water (a ubiquitous liquid of relatively low cost and high ease of disposal), a second- or third-generation high-index immersion fluid will require methods for recycle, so its costs can be spread over a larger number of wafers imaged. Therefore, we also discuss below the fluids' radiation durability and at-stepper recycle technology performance to permit these fluids' reuse.

3.1.1. Fluids at 157 nm. Studies of model small molecule fluids' photochemistry that were the focus of 157-nm pellicle radiation durability studies led to the development of 157-nm immersion fluid research. Various fluid classes were identified with low optical absorbance at 157 nm and with reasonable photochemical durability. These small-molecule fluids were therefore the initial candidates for 157-nm immersion fluids. We pursued broader-based studies on more than 50 candidate 157-nm immersion fluids to identify fluid classes appropriate for 157-nm imaging (67). These fluids' optical absorbances have both intrinsic and extrinsic contributions, so purification methods such as degasification, distillation, and supercritical fluid fractionation were investigated to determine residual contaminants' impact on absorbance. In most cases, the absorbance was dominated by dissolved oxygen and water in the fluid. Once these contaminant levels are reduced, the most transparent perfluoroether (PFE) measured was perfluoro-1,2-bis(2-methoxyethoxy)ethylene glycol (perfluorotriglyme), which has a 157-nm optical absorbance of 0.52 cm^{-1}; the most transparent perfluoroalkane (PFA) measured was perfluorohexane at 1.1 cm^{-1}; the most transparent hydrofluoroether (HFE) was 1-(1H-tetrafluoro)ethoxy-2-(1-trifluoromethyl)tetrafluoroethoxy-2-trifluoromethyl-1,1,2-trifluoroethane at 2.6 cm^{-1}; and the lowest projected absorption coefficient for a hydrofluoroalkane (HFA) was decafluoro-2H,3H-pentane at <2 cm^{-1}. Our chemical analysis showed that some impurities still remained in these materials, and so further reductions in absorption are possible. Even so, our current absorption values should allow lens-to-wafer working distances (assuming 95% transmission) of 428 nm, 203 nm, 83 nm, and 111 mm, respectively, for the four fluid classes. The identification of these four fluid classes (PFEs, PFAs, HFEs, and HFAs) for potential use as 157-nm immersion fluids—each with their own ranges of viscosity, vapor pressure, refractive index, dn/dT, synthetic routes, and cost—should allow for flexibility in performing trade-off analyses for various 157-nm immersion lithography engineering designs and cost-of-ownership estimates.

Because 157-nm "dry" lithography did not commercialize, the research in 157-nm immersion fluids stopped at this stage. From the following discussion of 193-nm immersion fluids, it is apparent that this research was only an initial step in defining an appropriately transparent fluid for 157-nm lithography. These fluids' indices, their radiation durabilities, their photochemical stabilities in use, and methods for recycle would all have required additional research.

3.1.2. Fluids at 193 nm. The largest NA for a water-based immersion scanner is the NA = 1.35 of the ASML XT:1950i shown in **Figure 1**; this projection lens has a dry NA ~ 0.93. Research on second-generation immersion fluids—whose 193-nm indices of 1.65 would enable scanners with NAs on the order of 1.55—requires identifying not just a high-index fluid with low 193-nm

optical absorbance, but also a fluid with high radiation durability and technology for fluid recycle and reuse at the stepper to meet the industry's fluid-cost-of-ownership goal of $1–2 per wafer level imaged. We discuss these aspects of immersion fluid research here.

3.1.2.1. Optical absorbance and refractive index. An immersion fluid's 193-nm refractive index is the source of the improved imaging possible. Other fluid properties are also critical to the successful fluid implementation in an immersion scanner. For comparison, water has a 193-nm refractive index at room temperature of 1.436 and a dn/dT of −90 ppm K^{-1} (68). Importantly, a fluid's optical absorbance will determine the working distance between the last lens element and the photoresist-coated wafer. For a 1-mm working distance (which is desired to assure high wafer productivity of >120 wafers h^{-1} and the requisite wafer-stage scanning speeds), the fluid must have a 193-nm optical absorbance of <0.1 cm^{-1}. The refractive index's temperature dependency is also a critical optical property: During use, the fluid's optical absorbance will lead to light absorption, and subsequent fluid thermal heating can lead to optical system imaging errors. There is a critical difference between an immersion fluid and the photoresist: The immersion fluid is an imaging material, which critically determines the projection lens' imaging performance. In other words, the fluid is comparable to the optical glass in the projection lens, insofar as what advantageous or deleterious effects the fluid can impart.

Many different immersion fluid classes have been studied (69) to identify materials and approaches for high-index and low-absorbance fluids, as summarized in **Figure 7** (34). Aqueous systems have utilized additives such as crown ethers (70), acids (71) (especially challenging for a production-worthy stepper!), and salts (72). Overall, the approach of using aqueous system additives does not achieve a large enough refractive index increase for a second-generation immersion fluid. The fundamentals of mixing can be studied using simple Lorentz oscillator models for interacting or noninteracting mixtures, and one finds that water's presence typically keeps the fluid's

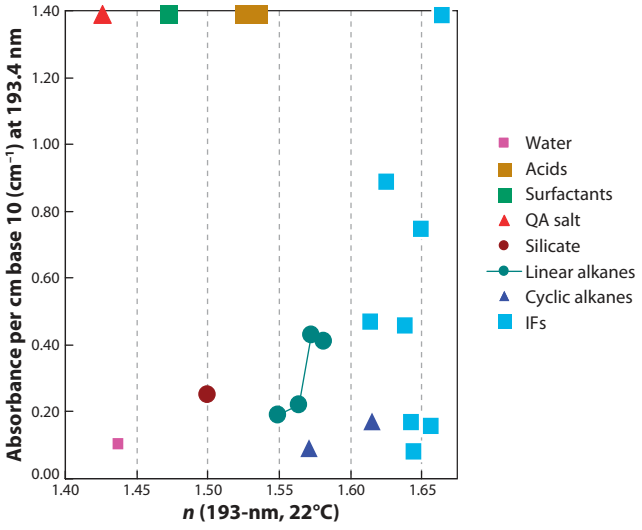

Figure 7

Refractive index and absorbance-cm^{-1} (base 10) of various categories of immersion fluid (IF) candidates at 193 nm. Fluids with absorbances above 1.4 cm^{-1} are shown at the top line in the property map. The second-generation fluid property goals are an index of refraction above 1.6 and an absorbance below 0.2 cm^{-1}. Adapted from Reference 34, with permission from SPIE.

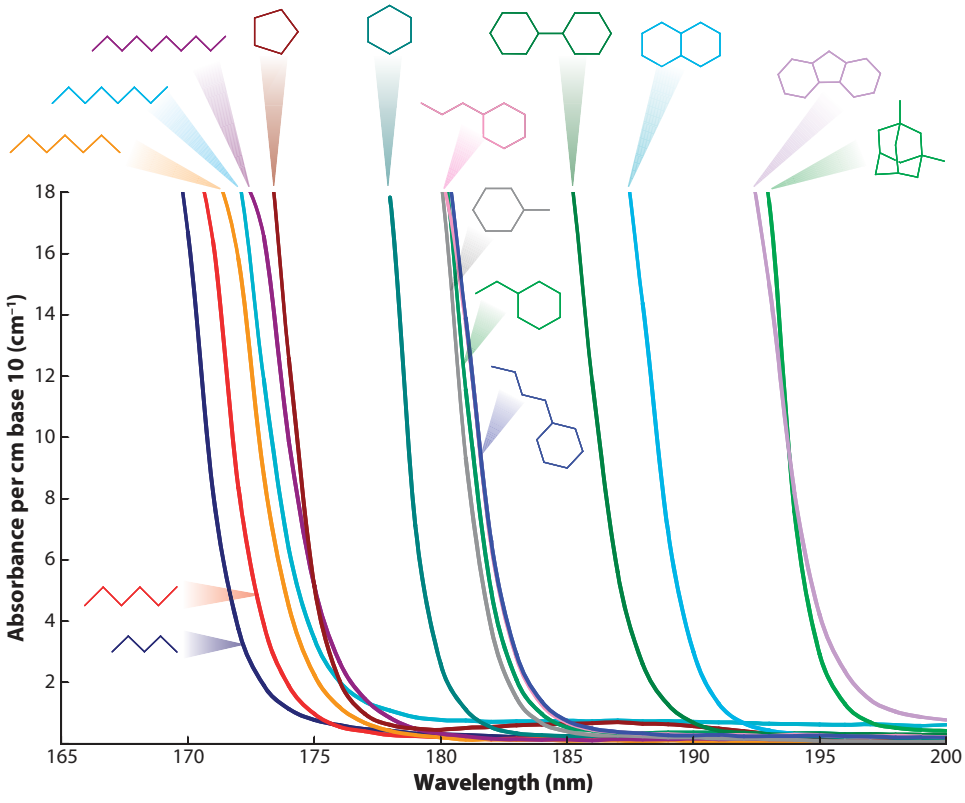

Figure 8

Optical absorbance-cm^{-1} (base 10) for various alkane immersion fluid candidates. Figure courtesy of Costner et al. (76). Adapted from Reference 34, with permission from SPIE.

193-nm index below approximately 1.58 (34). Organic fluids, such as the linear and cyclic alkanes, can achieve both the necessary high 193-nm index and the low 193-nm optical absorbance (73) and have been the focus of much study (74–77). Linear alkanes versus cyclic alkanes exhibit a lower refractive index for a comparable number of carbon atoms in the former, leading to a focus on the latter class. Costner et al. (76) show the trends in the optical absorption edge position for both linear and cyclic alkanes (**Figure 8**); as the number of carbon rings increases, the optical absorption edge shifts to longer wavelengths. There has also been work on nanoparticle approaches to third-generation fluids (78), and progress has been reported from fluids using high-index nanoparticles such as HfO_2.

One of the best second-generation immersion fluid candidates is IF132, which has optical absorbance at 193 nm $\sim$ 0.03 cm^{-1} (comparable to water's absorbance) and a 193-nm refractive index of 1.644. We also identified other fluids such as IF169 with an index of 1.656 and others with indices approaching 1.68 at 193 nm. It is instructive to compare the indices of water and IF132 (**Figure 9**): IF132 has an index at 589.3 nm (the sodium d-line wavelength) of 1.484, which is higher than water's index at this wavelength. If we define the index dispersion Δn as the difference in the index from 193 nm to 589 nm, then the dispersion of IF132 is 0.160, whereas water exhibits a dispersion of only 0.103. So in some ways, water is a rather low-index fluid, with relatively low dispersion when compared with second-generation immersion fluids. Another major difference

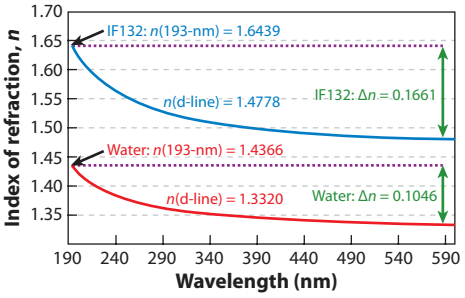

Figure 9

Spectral index of refraction versus wavelength of IF132 compared with water. Note IF132's increased n (d-line), dispersion Δn, and n (193 nm). Adapted from Reference 34, with permission from SPIE.

in the optical properties of water versus second-generation fluids is in the index temperature dependency. Here, water has an anomalously low dn/dT of -93×10^{-6} K^{-1}, whereas IF132 has $dn/dT = -550 \times 10^{-6}$ K^{-1}—an increase of more than $5\times$ (79). This fluid temperature dependency leads directly to a more accurate temperature control requirement in an immersion scanner using a second-generation fluid. It was also essential to study any other sources of variability in the fluids' optical properties. We therefore determined the variations of index, and $\Delta n/\Delta\lambda$ of IF132 and IF169, for different batches of fluid (within a 6-mo period), before-and-after irradiation (at 193.4 nm), before-and-after air exposure, and before-and-after resist exposure (image printing test). We found these changes to be not critical for system design.

3.1.2.2. Radiation durability and recycling. Following the development of viable second-generation immersion fluids such as IF132, it became essential to examine other property/process requirements relevant to commercial use, such as fluid radiation durability, last lens element contamination and cleaning, and (as discussed in the next section) resist interactions and profile effects. These studies show that both fluid handling issues as well as active fluid recycling must be well understood and carefully managed to maintain optimum fluid properties.

The radiation durability of second-generation immersion fluids, and their increased cost compared with the cost of water, requires that the fluids be recycled. A desirable approach is fluid recycle at the stepper, actively removing any photochemical degradation products during use—a process we call active recycle. The recycling methods' efficacy directly impacts the cost of ownership of high-index immersion lithography. It is therefore essential to develop a detailed understanding of radiation durability: how realistic exposure conditions (in a high-index immersion scanner) will impact both the immersion fluid and the scanner's last lens element. We have therefore developed detailed input and output metrics for both the fluids and the windows used in radiation durability tests, so these results can be cross-correlated to standard stepper conditions (80). Under such conditions, a typical fluid would be exposed to 6 J cm^{-2} in 1 week, and the last lens element would see a 60 kJ cm^{-2} dose per day. These magnitude differences are related to the fact that the fluid is circulating and the full fluid volume is not continuously irradiated, whereas the last lens element is continuously irradiated.

Using a fluid circulation system (**Figure 10**), we performed laboratory-scale experiments, in which the fluid was recirculated under 193-nm laser irradiation conditions mimicking the fluid's exposure in the standard stepper. Thus, the active-recycle system's efficiency in removing photodegradation products from the fluid could be determined in situ. We performed optical absorbance measurements on the laser irradiation cell, which determines the induced cell

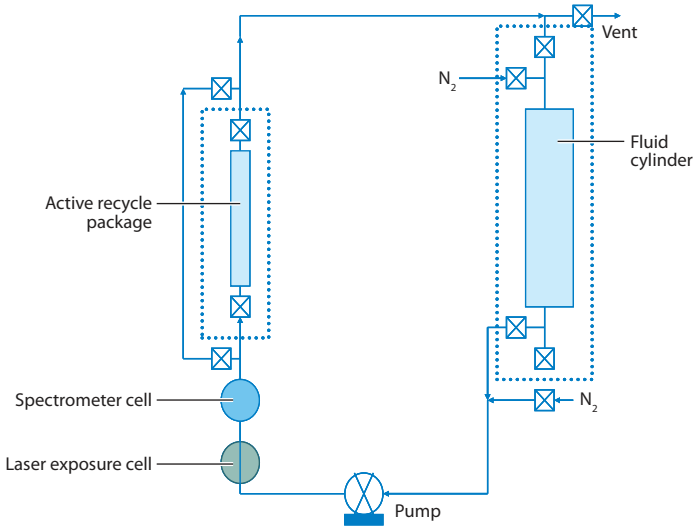

Figure 10

Schematic of the fluid circulation system. Figure adapted from Reference 80, with permission from SPIE.

absorbance, and on a second fluid absorbance spectroscopy cell, which determines the induced fluid absorbance. With these two results, we independently measured the fluid-induced absorbance rate and the window-induced absorbance rate to determine the rates of fluid and window darkening in use.

From a series of experiments, we determined the fluid's induced absorbance rate was 0.079 cm J^{-1} for IF132 without active recycle. The induced absorbance rate for other second-generation immersion fluids can be 50× to 100× higher than this IF132 result. Then, using two different active-recycle versions (versions 3 and 4), we found that the fluid's induced absorbance rate was decreased by a factor of 3× and 9× (**Figure 11**), leading to an increase in the fluid's usable life in the standard stepper to nine days.

In addition to the work on fluid recycling, there has been active fluid dynamics research on the fluid's flow over the wafer, under the projection lens. This research is useful both for issues such

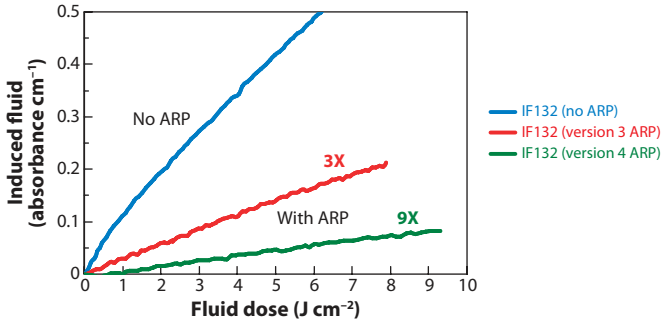

Figure 11

Induced fluid absorbance versus fluid dose for IF132, studied with no active-recycle package (ARP) and with two different versions that reduce the fluid's photochemical darkening rate by factors of 3× and 9× . These are averages of five experiments for each case.

as vibration control (81) and also for the possible introduction of fluid-flow-induced bubbles (or bubble entrapment from wafer topography), which can lead to imaging defects (82).

3.1.3. Immersion fluid–resist interactions. Using water or another higher-index-matching liquid between the last lens element and the photoresist introduces new issues not previously encountered in conventional dry lithography. Much of the early work identified the key issues related to imaging under water immersion (83), and later, the same issues were addressed for the higher-index organic liquids (84). Of particular concern is the extent of resist components' extraction from the resist film into the immersion liquid. Components in the resist formulation such as PAGs and their photogenerated acids, dissolution modifiers, and bases may all leach from the film. The amount of leaching is of course a function of the resist film's component concentration, the rate of the components' diffusion into the liquid, the solubility of the components, and the time of fluid/resist contact. Leaching has two effects. First, the resist's imaging properties, such as sensitivity, are changed, and performance is usually degraded. Second, leached components, especially PAGs, may undergo further photochemistry and adsorb onto the system optics (85, 86), a topic of particular concern to the stepper manufacturers—which has led to their setting maximum tolerable PAG limits on the order of $1.0–5.0 \times 10^{-12}$ mol $(cm^2\text{-}s)^{-1}$. The PAG amount detected in water for some commercially available resists has either come very close to or exceeded this limit (87–90). This result has prompted further work on designing immersion topcoats or topcoatless resists (vide infra) to slow or prevent leaching. It has also led to work to prerinse the resist surface with water [because most of the PAG leaching occurs in the first few seconds of contact (91)], which has been reported to remove more than 90% of the PAG at the water-resist interface. With second-generation immersion fluids, very little PAG leaching has been detected, reportedly approximately two orders of magnitude lower than the recommended limit (see **Figure 12**).

Another key immersion imaging issue is the effect of fluid penetration into the resist film. Subsurface immersion liquid may modify the kinetics of the acid-catalyzed deprotection reaction (especially if water carries with it species that can quench photoacid). It can also act as a polymer film plasticizer (especially true for organic liquids diffusing into organic resist polymers), changing the film's mechanical properties and diffusion-related properties. With water as the immersion fluid, quartz crystal microbalance and optical reflectance techniques have shown that 200-nm

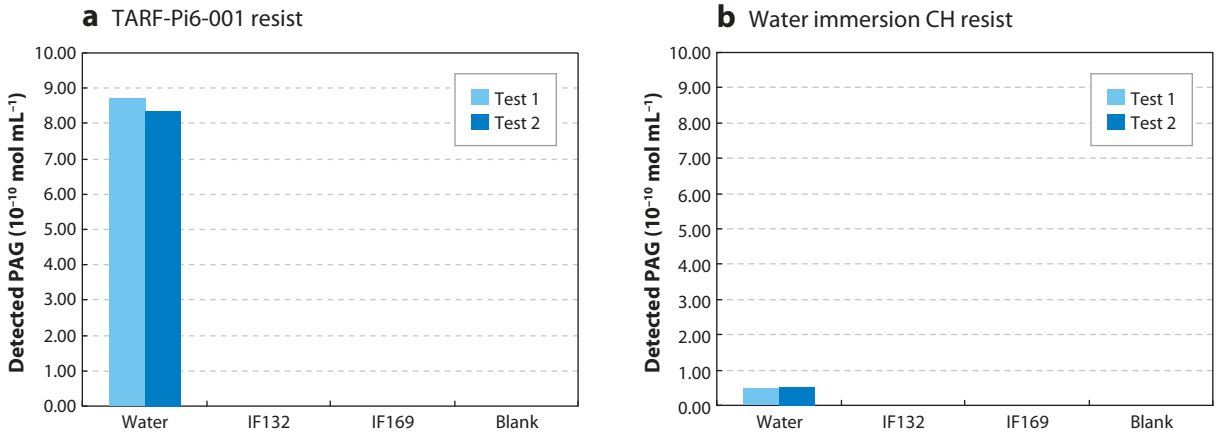

Figure 12

Amount of photoacid generator (PAG) leached in 6 min from two water-specific immersion resists into IF132 and IF169. No PAG was detected in the high-index liquids.

films may swell up to 5 nm in thickness (83). There is also some evidence that second-generation immersion fluids cause up to 2 nm in initial swelling, and up to 10 nm of dissolution, of some commercial resists (84). Despite these observations, there seem to be only subtle effects on sub-45-nm line and space interference imaging of some commercially available resists with both water and second-generation immersion fluids (vide infra).

Both resist component extraction into the immersion fluid, and fluid permeation into the resist, may cause unwanted defects in the final resist image, and much work has been done to quantify and reduce the new defect types seen under immersion imaging (92–94). These defect types may be classified into five general categories: process-induced defects, watermark defects, defects arising from bubbles in the fluid, drying stain defects, and particle-borne defects. Defects related to processing may originate from fluid-carrying particles from the wafer edge, especially if the topcoat, resist, or BARC peels at the edge, and the fluid is scanned beyond this edge point. Steps to rinse and clean the bevel have shown marked improvement in defect counts. Fluids that permeate into the resist film can generate watermark defects, which include swelling of lines and T-topping. Bubbles (which may originate from gaseous by-products from the resist or entrapment of bubbles from fast scanning at the advancing edge of the fluid-resist interface) may be a source of undeveloped resist regions. Resist component leaching into the fluid, in conjunction with fluid droplet evaporation, may lead to drying stain defects. Drying stain defects are also possible if the fluid is not pure, with evaporation leading to surface residues. Finally, fluid or environmental particles can cause printed defects if present during exposure. Optimization in both processing and immersion-related materials is necessary to improve defect performance. These improvements have resulted in defect densities below 0.06 cm^{-2} for water immersion. For high-index immersion, preliminary defect studies have concentrated on both the high-index fluids, cleanliness and fluid-misted droplets' interaction with several commercially available dry and water immersion photoresists (95). Misted defect counts of a high-index fluid, designated IF132, have shown acceptable numbers for further optimization. Experiments in which the resist is soaked with the fluid before and after exposure show that the printed 90-nm lines do not vary significantly in lateral line dimension, with only a slight resist thickness loss.

3.2. Immersion Topcoats and Photoresists

Although some topcoats and photoresists for dry lithography can be used, optimal imaging performance is only obtained when these materials are specifically optimized for immersion imaging. In this section, research on novel topcoats, topcoatless photoresists, and high-index photoresists for third-generation immersion lithography are discussed.

3.2.1. Topcoats and topcoatless photoresists. Fears of lens contamination, increased defects, and resist performance degradation with water immersion lithography prompted much research activity on novel topcoats and the so-called topcoatless photoresists. Topcoats are designed to reduce both water permeation into the photoresist as well as resist component leaching (especially PAG) and also to increase water's receding contact angle at fast scan speeds (to reduce water droplet formation that may lead to imaging defects). More hydrophobic topcoats provide the increased receding contact angle to allow higher scanning velocities before droplet formation occurs (82). Topcoats showing more than 100° receding contact angles will enable speeds up to 900 mm s^{-1}. Ideally, the topcoat would dissolve in the same aqueous base developer (TMAH) used in the resist development step, but some topcoat versions were designed for nonaqueous solvent development, which adds an extra processing step. Many topcoats incorporate fluorine-containing functional groups for their increased hydrophobicity, as well as the same compound

types used effectively for absorbance reduction in 157-nm technology (88, 96–101). These fluoropolymers have also been used in water immersion resist materials—either as additives to current 193-nm materials or as block copolymers (102–104). These systems are designed so that a topcoat is not necessary, but instead incorporate the topcoat's hydrophobic properties directly into the photoresist, eliminating an extra topcoat spinning step. These topcoatless resists depend on the self-segregation of low-surface-energy fluoro-components to the air interface during spinning and baking, providing the needed hydrophobicity for water immersion imaging. A novel method to make the block copolymers relies on RAFT polymerization to make the first block composed of 193-nm photoresist monomers, followed by a second block composed of a fluorinated monomer. Blends of this block copolymer (even at very small fractions) with a standard nonfluorinated methacrylate terpolymer show high receding contact angles. One variant to this system, which may further reduce the defect levels, involves modifying the fluorinated block to be developer soluble—which would also help with developer wettability.

3.2.2. High-index photoresists for third-generation immersion. Current 193-nm photoresists have refractive indices of approximately 1.7, which would be the limiting index in the optical path if a higher-refractive-index fluid (~1.8) and LuAG (lutetium aluminum garnet, with a 193 nm index of 2.14, as the last lens element) were used. Thus, there has been some research effort to predict, screen, and synthesize materials possessing both a target refractive index of 1.9 and the required absorbance below 3 μm^{-1} (105, 106). Quantitative structure property relationship (QSPR) modeling was developed from a database of hundreds of organic compounds to predict refractive indices at 589 nm (107). This information, along with knowledge of the refractive index dispersion, was used to show that molecules with high molecular weight, high heat of formation, high sulfur contents, and low fluorine and hydrogen contents increase refractive index at 193 nm. Other researchers have taken this information to design and synthesize imageable resist polymers containing thioacetal, thioester, and sulfone groups, with absorbance edges near 193 nm [for both high refractive index and low absorption (108)]. One particular copolymer, incorporating both an adamantyl methacrylate as well as a methacrylate having both a thioester and sulfone functionality, has a refractive index above 1.8 and an absorbance below 1.4 μm^{-1} and was successfully imaged to produce 110-nm lines and spaces.

4. IMMERSION LITHOGRAPHY IMAGING PERFORMANCE AT 193 NM

4.1. Comparative Water and Second-Generation Fluid Imaging

In this section, we highlight work done to compare water-based and high-index fluid-based imaging. Because no water immersion tools were available early in immersion development, researchers relied on soaking experiments to provide a sense of the imaging capability of the most current 193-nm dry resists, using production-worthy dry 193-nm tools. The resist films were soaked with water before and after exposure and then processed normally (88, 109). The same experiments were performed using high-index fluids, and the 90-nm resist profiles were compared (using scatterometry metrology) for each fluid on three commercially available resists: a dry line-space resist, a water immersion line-space resist, and a water immersion contact hole resist (**Figure 13**). Each fluid had its own subtle effects on each resist. For example, water tended to provide thicker and wider resist profiles on the dry resist (presumably owing to resist component extraction such as PAG), but the same effect was lessened on a water immersion–dedicated resist. The high-index fluid IF132 was observed to thin the resist profiles after postexposure soak. Although the resist profiles were affected by direct fluid contact, researchers concluded that the improvements made

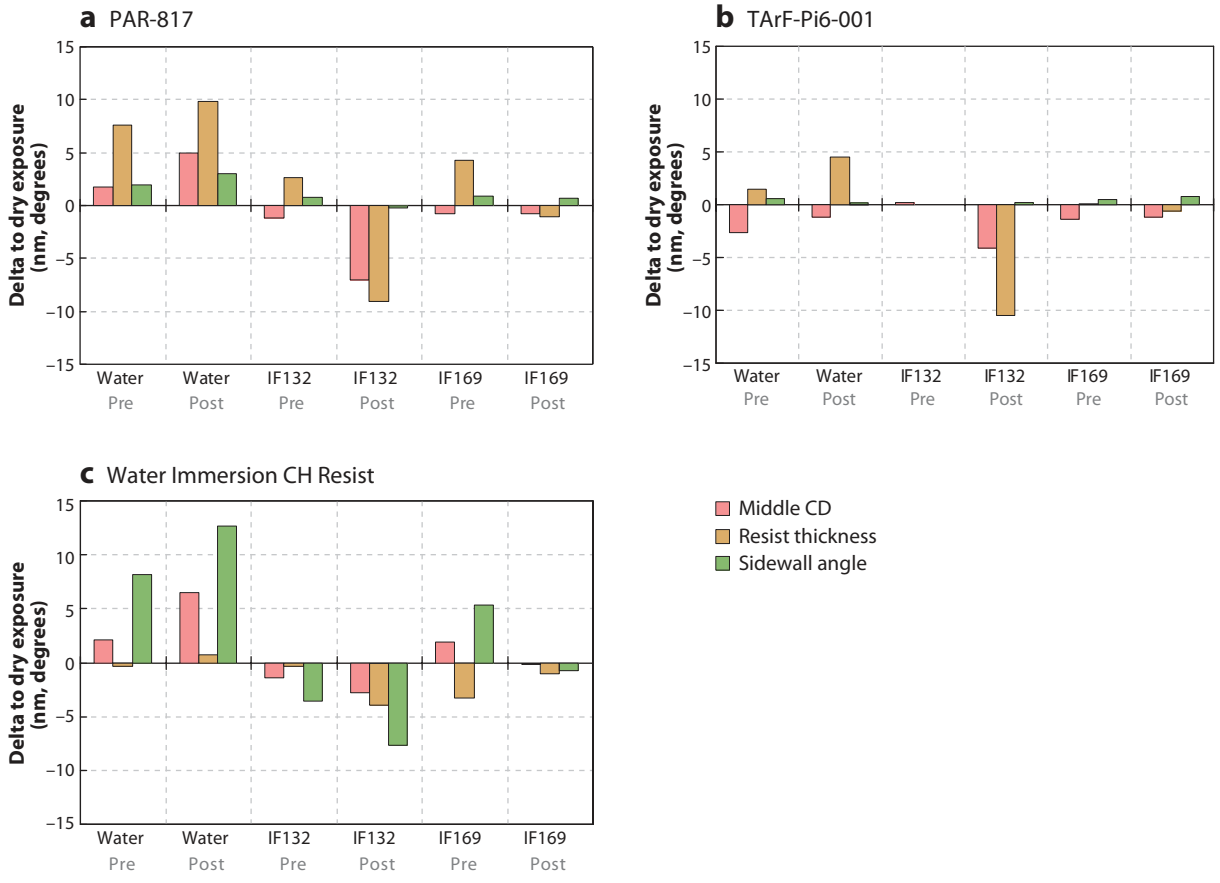

Figure 13

Delta between scatterometry parameters for a dry reference wafer and wafers soaked preexposure (pre) or postexposure (post).

in the most current water immersion–dedicated resists also had a positive effect on the high-index fluids' imaging.

4.2. Interference Imaging

Interference imaging printers have long been available but now have a new use: a rapid, cost effective way to develop immersion lithography, particularly at extremely high resolutions. Although interference printers will never replace classical lens-based lithography systems for semiconductor device production, they do offer a means to develop resist and fluid technology at relatively low cost. Their simple image-forming format (shown in **Figure 14** for dual-beam interference imaging) offers easy access to the basic physics of advanced imaging. Issues such as polarization of the image-forming light rays, fluid-resist interaction during exposure, topcoat film performance, and resist LER at extremely high resolutions can all be readily studied.

Interference printing of several commercial resists that are fully submersed in either water or a high-index fluid during exposure has been demonstrated, providing resolutions beyond current lens-based system capabilities (95, 109–111). In early development, lines with dimensions as low

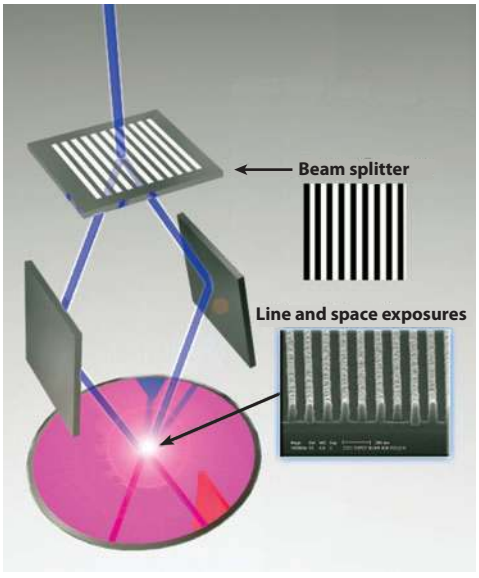

Figure 14

Two-beam interferometric imager. Sin(θ) and hence resolution are set by adjusting the positions and angles of the mirrors. Adapted from Reference 34, with permission from SPIE.

as 32 nm were printed using a dry, commercially available resist submersed in IF132 in a two-beam interferometer (112). In later experiments, 36-nm half-pitch lines were printed to directly compare water immersion imaging and high-index immersion imaging (because water immersion allows only printing of half pitches down to 34 nm on the basis of current processing optimizations with NA of 1.35). **Figure 15** shows the top-down and cross-sectional scanning electron micrographs (SEMs) of the lines obtained for one dry (PAR-817) and two water immersion–dedicated resists using water and two high-index fluids. The improvements made for the water immersion resists were evident in the imaging: Clean 36-nm lines and spaces were obtained under water as well as under the two high-index fluids. Lines with dimensions as small as 29 nm were even obtained with the two immersion-dedicated resists using IF132 as the immersion fluid (**Figure 16**). These imaging tests demonstrate the great strides made in resist performance and the compatibility of commercially available resists with both water and high-index fluids; with further process and material optimizations, line dimensions to 32 nm can be printed with the higher-index fluids.

5. DOUBLE-PATTERNING METHODS

Strategies to further increase resolution by optical means alone may have been exhausted because decreasing the wavelength beyond 193 nm leads to EUV lithography, a nonoptical method that has several major unresolved problems. Also, increasing the NA to 1.55 with high-index fluids will allow patterning down to only 32-nm half pitch, even at the most aggressive k factors. The most likely alternative would be some form of double patterning, in one variation of which the desired patterns are split between two masks, such that more facile feature printing is done at twice the pitch. The second mask would be aligned so that the second feature set is printed between the first set, providing final features with target dimensions at the desired half pitch. This takes advantage of the fact that one can image smaller features more easily if the pitch is

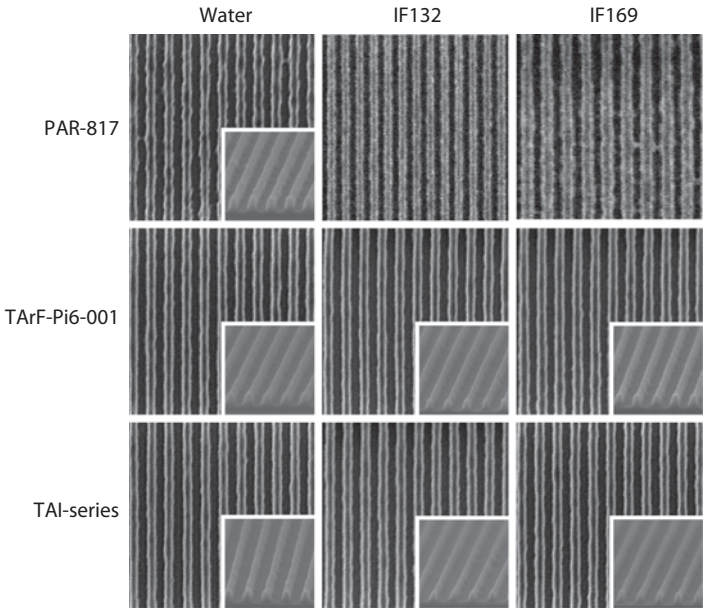

Figure 15

Top-down and cross-sectional scanning electron micrographs (SEMs) of 72-nm pitch lines imaged on a two-beam interferometer under three liquids on three resists.

relaxed (the features are spaced farther apart) because the spatial frequency of each of the two images printed is reduced when compared with a single exposure half pitch to make the same dense features. For example, if one wanted to print 30-nm lines and spaces, one would start by printing 30-nm lines with 90-nm spaces and then print another set of 30-nm lines with 90-nm spaces over the original image but align the exposures with a 60-nm offset (113). One can envision that the costs associated with double-patterning lithography would be substantial, given the extra processing steps and materials required. However, because EUV lithography has missed several target development times, and optical lithography with water or high-index fluid immersion has

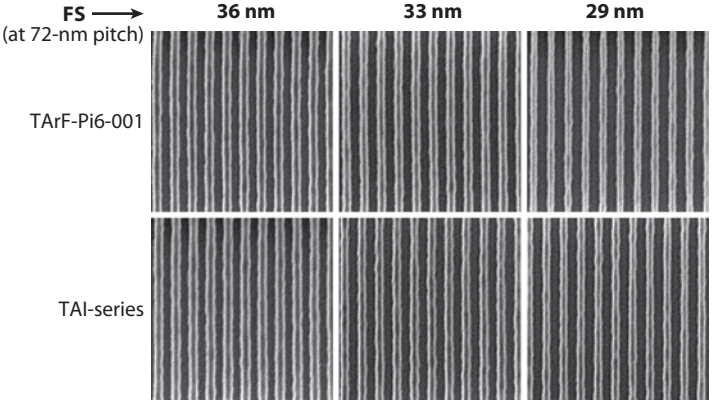

Figure 16

Top-down scanning electron micrographs (SEMs) of 72-nm pitch lines imaged using IF132 on a two-beam interferometer as a function of increasing exposure dose from left to right. FS, feature size.

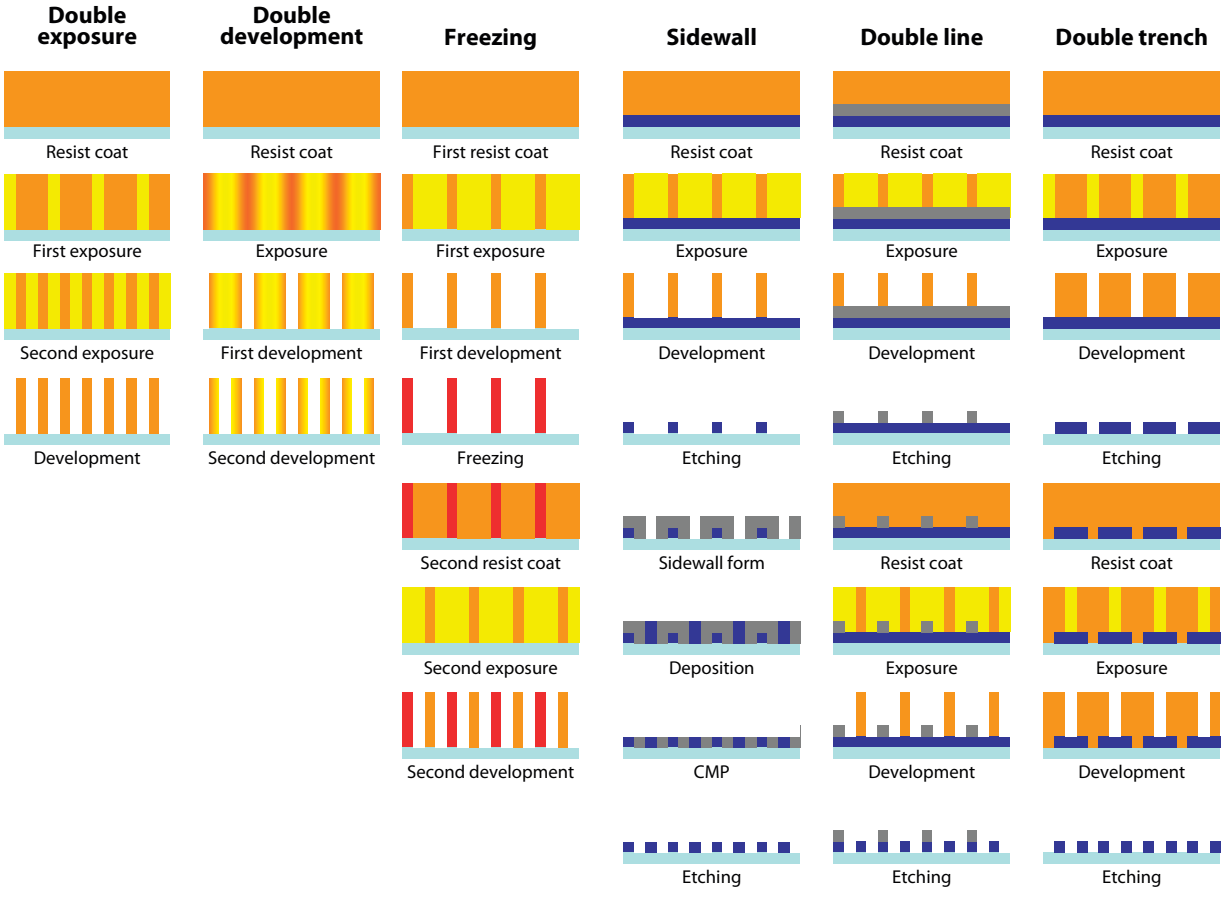

Figure 17

Approaches for double-patterning lithography. Approaches increase in complexity of processing steps from left to right: The least complex (but most material-demanding) approach is at the left, and the most complex process (but least material-demanding) approach is at the right. CMP, chemical mechanical planarization or chemical mechanical polishing. Figure from Tarutani-san, Fujifilm. Adapted from Semiconductor International Webcast on Preparing for High-Volume Immersion Lithography (121).

shown much potential, applying some double-patterning method to immersion lithography would provide a means to further resolution improvements to keep pace with integrated circuits' leading-edge feature size requirements.

Several industrial laboratories and academic institutions are developing their own approaches for accomplishing this double-patterning task. **Figure 17** schematically shows a few such approaches (114). The last two columns depict the double-patterning method described above, in which two exposure steps, two development steps, and two etching steps are required for pitch doubling. This method's costs have prompted researchers to scout other alternatives that could eliminate some of the extra processing steps. The most challenging approach is a double-exposure method shown in the first column of **Figure 17**. In this method, the two mask patterns are exposed consecutively into the same material, providing better overlay accuracy (because the wafer is not removed from the scanner chuck). This requires a material that can behave in an optically nonlinear manner, and to date no such material exists, although some conceptual and simulation work has been reported (115–118). The material must "forget" subthreshold exposure doses in the first

exposure pass before the second one; otherwise, the two individual mask images are not resolved. Many current photosensitive materials possess this memory effect: Subthreshold exposure in the first pass reduces the dose required for chemical change in the second one. First-order phase transitions, in contrast, show no memory effect because the same energy amount is required to heat a material to the melt transition the second time after it has been cooled from the first heat—the transition is reversible. Several material approaches to obtain a nonlinear response to exposure have been proposed. One of the more interesting concepts is the photoreversible topcoat, or what is termed the contrast enhancement layer (CEL). The CEL is a thin layer of opaque material on top of a conventional photoresist that is rapidly photobleached when illuminated at 193 nm in the first exposure pass and then regains its opacity after illumination before the second pass. In effect, this topcoat would act as a reversible contact mask, allowing light to penetrate in regions where aerial image intensities are higher than the threshold and preventing light penetration in regions where the aerial image intensities are lower. Photochromic molecules are good candidates for this purpose and, depending on their chemistry, can undergo reversion by relaxation, thermal, or optical means. For example, spiropyrans and spirooxazines are colorless in the leuco form but become colored after irradiation, reverting back to the leuco form with heat. Other molecules like the diarylethenes can revert back to the original form via visible light. Work is under way to identify photochromic systems that are effective at 193 nm, because most known systems are active at wavelengths greater than 300 nm. This may not be an easy task because some of the other desired CEL properties may be difficult to achieve. Such desirable properties include fast film bleaching with a transmission optical density of 2.0 to a stable saturated optical density of 0.2, using approximately 30 mJ cm^{-2} of 193-nm radiation; fast reversion once illumination is stopped; spin coatability over current photoresists; and the capacity for development in a standard photoresist developer.

Two other approaches for double patterning are termed double development (or dual-tone development) and resist freezing. In double development, a hybrid resist (which is essentially a mixture of a positive-tone resist and a negative-tone resist) that exhibits two solubility transitions at the optimal exposure dose is used (119–121). As the initially insoluble hybrid resist is exposed, it reaches a threshold dose at which it becomes soluble in TMAH developer (a positive-tone characteristic). At higher-exposure doses, the resist reaches another threshold point at which it becomes insoluble in solvent (a negative-tone characteristic). One must therefore match the two threshold points to formulate a resist that provides pitch doubling from the sinusoidal aerial image. The hybrid resist would transform at intensities higher than the threshold in a positive-tone development step and would transform at intensities lower than the threshold in a negative-tone development step (**Figure 18**) (122). The resist is insoluble at intensities between the two thresholds. Double development may be a promising method to achieve pitch doubling (and can be done with only one exposure) but would most likely be useful only for uniformly periodic structures, so this approach will not find general use (for logic devices in particular).

Resist freezing (123–125) requires two coating and two development steps, and the wafer must leave the exposure chuck to undergo a freezing process, which may involve coating the freezing material over the first developed image—with a subsequent bake to freeze the image (cross-linking chemistry) that renders it insoluble in an aqueous base developer. The freezing material is removed, and the second resist coat, exposure, and development steps are performed to obtain the desired double pattern. Each industrial company has its own method to accomplish the freezing or cross-linking step. In one example, photoresists that contain the lactone functionality are modified by vapor-deposited diamines as a cross-linker (123).

A final alternative uses a self-aligned double-patterning (SADP) technique, or sidewall spacer technique, to achieve pitch doubling (126–129). In this process, shown schematically in

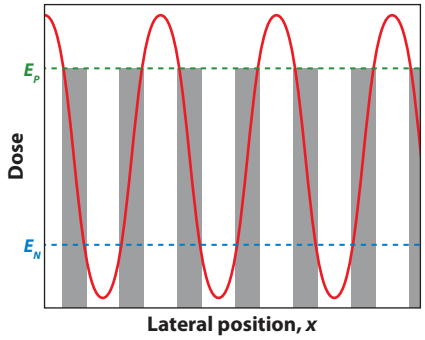

Figure 18

Pitch doubling from a hybrid resist, in which both positive-tone (E_P) and negative-tone (E_N)thresholds are used. White areas are soluble in developer, whereas light brown areas are insoluble. Adapted from Semiconductor International Webcast on Preparing for High-Volume Immersion Lithography.

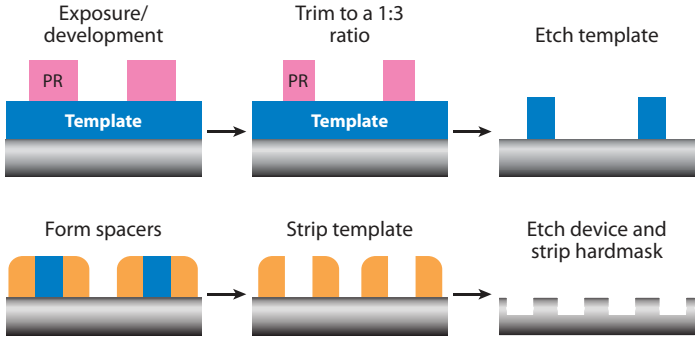

Figure 19

Generic process flow for positive-tone spacer mask patterning. Adapted from Reference 126, with permission from Chris Bencher.

Figure 19, the first optical exposure pattern is etched into a sacrificial layer. Another material (e.g., silicon nitride) is then deposited conformally onto this spacer's sides to a thickness that defines the final pattern. In positive-tone spacer processes, the first sacrificial layer is removed, and the pattern formed by the deposited material is etched into the final hardmask or substrate. Excellent-quality lines down to 22-nm half pitch have been obtained. Although this process involves only a single resist application, it does add a number of process steps, contributing to the approach's complexity. As with the double-development approach, this technique may not find general use because it is applicable only to uniformly periodic structures.

6. CONCLUSION, NEEDS, AND CHALLENGES

This review of immersion lithography materials research defines both the critical application requirements and the nature and properties of the materials that have been developed and commercialized into today's production immersion lithography. It also discusses the many different materials, approaches, and technologies that have been the subject of considerable research and development but that were not successfully commercialized. In addition, we show how the advances in materials science developed; even the "failed" technology research efforts, have been critical to the successful technological developments that followed them. For example, one overarching

theme is the development of an in-depth understanding of the intrinsic and extrinsic contributions to both the optical absorbance and the refractive index (or, more generally, the complex index of refraction) of inorganic, polymeric, and molecular materials in the UV and vacuum UV spectral regions. This deep scientific basis of understanding underlies all efforts at addressing future technological needs through the successful development and commercialization of optimized materials and technology.

SUMMARY POINTS

1. Given the complexity of introducing a new lithographic wavelength, the integrated-circuit (IC) industry is seeking to extend its current leading-edge 193-nm lithography, using a number of material and optical enhancements.
2. Immersion lithography—first with water, and potentially later with higher-refractive-index fluids—has been a key technology in extending 193-nm lithography.
3. Lithography at 193 nm has been enabled and extended by advanced phase-shifting photomasks and by the pellicles used to protect them from surface contamination during use.
4. Immersion lithographic technology has placed new demands on photoresists, and such demands may increase in the future with the adoption of the various double-patterning options.
5. Double-patterning technologies are emerging but are not yet mature because the optimum options in terms of both materials and processes are still in development.

FUTURE ISSUES

1. Immersion lithography could be significantly extended by fluids with refractive indices >1.8, combined with high transparency at 193 nm and good photochemical durability.
2. The need for a separate topcoat could be eliminated by development of photoresists compatible with immersion fluids.
3. Future IC technologies will require photoresists with refractive indices of at least 1.9, and acceptable absorbance levels.
4. Optimized polymers will facilitate nanoimprint applications.
5. Double-patterning applications require advanced photoresists and other polymers (including photoactive ones).

DISCLOSURE STATEMENT

The authors are not aware of any biases that might be perceived as affecting the objectivity of this review.

ACKNOWLEDGMENTS

The authors would like to acknowledge Franklin Kalk and Craig West of Toppan Photomasks Inc., Jan Mulkens and Harry Sewell of ASML Inc., and Eric Lin of the National Institute of Standards and Technology (NIST) for helpful discussions, and Michael Mocella of DuPont and

Barbara French for editing the manuscript. Some portions of the work presented here were supported with funding from International Sematech and the National Science Foundation.

LITERATURE CITED

1. Reichmanis E, Novembre AE. 1993. Lithographic resist materials chemistry. *Annu. Rev. Mater. Sci.* 23:11–43
2. Deal BE, Crossley PA. 1981. Microstructure fabrication in electronic devices. *Annu. Rev. Mater. Sci.* 11:321–51
3. Rayleigh RS. 1896. On the theory of optical omages, with special reference to the microscopy. *London, Edinburge, Dublin Philos. Mag. J. Sci.* 42(255, Pt. XV):167–95. Reprinted in Ref. 130, p. 51
4. Lin BJ. 2002. The k_3 coefficient in nonparaxial λ/NA scaling equations for resolution, depth of focus and immersion lithography. *J. Microlithogr. Microfabr. Microsyst.* 1:7–12
5. Moore GE. 1965. Cramming more components onto integrated circuits. *Electronics* 38(8):114–17. Reprinted in Ref. 130, p. 175
6. Moore GE. 1975. Progress in digital integrated electronics. Int. Electron Devices Meet. 1975 Tech. Digest, pp. 11–13. Reprinted in Ref. 130, p. 179
7. Moore GE. 1995. Lithography and the future of Moore's Law. *Optical/Laser Microlithogr. VIII*, ed. TA Brunner, Proc. SPIE Vol. 2440, pp. 2–17. Reprinted in Ref. 130, p. 182
8. Solomon PM. 2000. Device innovation and material challenges at the limits of CMOS technology. *Annu. Rev. Mater. Sci.* 30:681–97
9. Howard RE, Skocpol WJ, Jackel LD. 1986. Nanostructures. *Annu. Rev. Mater. Sci.* 16:441–66
10. Sewell H, Mulkens M. 2009. Materials for lithography. *Annu. Rev. Mater. Res.* 39. In press
11. Xia Y, Whitesides GM. 1998. Soft lithography. *Annu. Rev. Mater. Sci.* 28:153–84
12. Costner EA, Lin MW, Jen W-L, Willson CG. 2009. Nanoimprint lithography materials development for semiconductor device fabrication. *Annu. Rev. Mater. Res.* 39. In press
13. Gate BD, Xu Q, Love JC, Wolfe BD, Whitesides GM. 2004. Unconventional nanofabrication. *Annu. Rev. Mater. Res.* 34:339–72
14. Ross CA. 2001. Patterned magnetic recording media. *Annu. Rev. Mater. Res.* 31:203–35
15. Dammel RR. 2002. Photoresists for microlithography, or the Red Queen's race. *J. Microlithogr. Microfabr. Microsyst.* 1:270–75
16. Thompson LF, Kerwin RE. 1976. Polymer resist systems for photo- and electron lithography. *Annu. Rev. Mater. Sci.* 6:267–301
17. Reichmanis E, Thompson LF. 1987. Polymer materials for microlithography. *Annu. Rev. Mater. Sci.* 17:235–71
18. Russell TP. 1991. Characterization of polymer interfaces. *Annu. Rev. Mater. Sci.* 21:249–68
19. Pawloski AR, Acheta A, Levinson HJ, Michaelson TB, Jamieson A, et al. 2006. Line edge roughness and intrinsic bias for two methacrylate polymer resist systems. *J. Microlithogr. Microfabr. Microsyst.* 5:023001
20. Lin EK, Soles CL, Goldfarb DL, Trinque BC, Burns SD, et al. 2002. Direct measurement of the reaction front in chemically amplified photoresists. *Science* 297:372–75
21. Kang S, Vogt BD, Wu WL, Prabhu VM, VanderHart DL, et al. 2007. Characterization of compositional heterogeneity in chemically amplified photoresist polymer thin films with infrared spectroscopy. *Macromolecules* 40:1497–503
22. Lenhart JL, Jones RL, Lin EK, Soles CL, Wu WL, et al. 2002. Probing surface and bulk chemistry in films using near edge X-ray absorption fine structure. *J. Vac. Sci. Technol. B* 20:2920–26
23. Vogt BD, Kang S, Prabju VM, Lin EK, Satija SK, et al. 2006. Measurements of the reaction-diffusion front of model chemically amplified photoresists with varying photoacid size. *Macromolecules* 39:8311–17
24. Hohle C, Heckmann N, Sebald M, Markert M, Stepanenko N, et al. 2005. Surface roughness investigation of 157- and 193-nm polymer platforms using different etch conditions. *J. Microlithogr. Microfabr. Microsyst.* 4:043009
25. Steenwinckel DV, Gronheid R, Roey FV, Willems P, Lammers JH. 2008. Novel method for characterizing resist performance. *J. Microlithogr. Microfabr. Microsyst.* 7:023002

26. Brunner TA. 2003. Why optical lithography will live forever. *J. Vac. Sci. Technol. B* 21:2632–37
27. Trybula WJ. 2005. Status of 157-nm optical lithography. *J. Microlithogr. Microfabr. Microsyst.* 4:0111007
28. Rothschild M, Bloomstein TM, Kunz RR, Liberman V, Switkes M, Palmacci ST. 2004. Liquid immersion lithography: why, how and when? *J. Vac. Sci. Technol. B* 22:2877–81
29. Zell Th. 2006. Present and future of 193 nm lithography. *Microelectron. Eng.* 83:624–33
30. Lin BJ. 2004. Immersion lithography and its impact on semiconductor manufacturing. *J. Microlithogr. Microfabr. Microsyst.* 3:377–95
31. Mulkens J, Flagello D, Streefkerk B, Graeupner P. 2004. Benefits and limitations of immersion lithography. *J. Microlithogr. Microfabr. Microsyst.* 3:104–14
32. Owa S, Nagasaka H. 2004. Advantage and feasibility of immersion lithography. *J. Microlithogr. Microfabr. Microsyst.* 3:97–103
33. McCallum M, Kameyama M, Owa S. 2006. Practical development and implementation of 193 nm immersion lithography. *Microelectron. Eng.* 83:640–42
34. French RH, Sewell H, Yang MK, Peng S, McCafferty D, et al. 2005. Imaging of 32-nm 1:1 lines and spaces using 193-nm immersion interference lithography with second-generation immersion fluids to achieve a numerical aperture of 1.5 and a k_1 of 0.25. *J. Microlithogr. Microfabr. Microsyst.* 4:031103
35. Bloomstein TM, Fedynyshyn TH, Pottebaum I, Marchant MF, Deneault SJ, Rothschild M. 2006. Immersion patterning down to 27 nm half pitch. *J. Vac. Sci. Technol. B* 24:2789–97
36. Lin BJ. 2006. The ending of optical lithography and the prospects of its successors. *Microelectron. Eng.* 83:604–13
37. Wojcik GL, Mould J, Ferguson RA, Martino RM, Low KK. 1994. Some image modeling issues for I-line, 5× phase-shifting masks. *Proc. SPIE* 2197:455–65
38. Schellenberg FM, Adam K. Matteo J. Hesseling L. 2005. Electromagnetic phenomena in advanced photomasks. *J. Vac. Sci. Technol. B* 23:3106–15
39. Chien P, Chen M. 1987. Proximity effects in submicron optical lithography. In *Optical Microlithography VI*, ed. HL Stover, Proc. SPIE Vol. 772, pp. 35–40. Reprinted in Ref. 130, p. 260
40. Lin BJ, Moruzzi AM, Rosenbluth AE. 1990. Lithographic process having improved image quality. *US. Patent No. 4,902,899*. Reprinted in Ref. 130, p. 296
41. Hikichi R, Ishii H, Migita H, Kakehi N, Shimizu M, et al. 2008. Photomask technology for 32 nm node and beyond. *Proc. SPIE* 7028:702805
42. Kojima Y, Shirasaki M, Chiba K, Tanaka T, Inazuki Y, et al. 2007. Alternating phase-shift mask and binary mask for 45-nm node and beyond: the impact on the mask error control. *Proc. SPIE* 6607:66070C
43. Philipsen V, Bisschop PD, Mesuda K. 2008. Mask transmission resonance in bi-layer masks. *Proc. SPIE* 7028:702815
44. Hashimoto M, Iwashita H, Kominato A, Shishido H, Ushida M, Mitsui H. 2008. The ultimate chrome absorber in photomask-making. *Proc. SPIE* 7028:702804
45. Takagi M, Mizoguchi T, Kojima Y, Saga T, Haraguchi T, et al. 2007. Improvement of CD variation control for attenuated phase-shift mask. *Proc. SPIE* 6607:66070B
46. Erdmann A, Fühner T, Evanschitzky P. 2008. Optimization of mask absorber stacks and illumination settings for contact hole imaging. *Proc. SPIE* 7028:70283L
47. Zavyalova L, Songa H, Lucas K, Zhanga Q, Shiely J. 2008. Modeling mask pellicle effects for OPC/RET. *Proc. SPIE* 7028:70283B
48. Racette K, Watts A, Barrett M, Nolan R, Sasaki Y, et al. 2007. *Proc. SPIE* 6607:66071V
49. Konishi T, Kojima Y, Takahashi H, Tanabe M, Haraguchi T, et al. 2008. MoSi absorber photomask for 32 nm node. *Proc. SPIE* 7028:702803
50. Montgomery PK, Litt LC, Conley W, Lucas K, Van Wingerden, Wiaux V. 2004. Comparison of 9% and 6% transmission attenuated phase shift mask for the 65 nm device node. *J. Microlithogr. Microfabr. Microsyst.* 3:276–83
51. Kalk FD, French RH, Alpay HU, Hughes G. 1994. Attenuated phase shifting photomasks fabricated from Cr-based embedded shifter blanks. *SPIE* 2254:64–70
52. Johs B, French RH, Kalk FD, McGahan WA, Woollam JA. 1994. Optical analysis of complex multilayer structures using multiple data types. *SPIE* 2253:1098–106

53. Alpay U, French RH, Kalk F. 1995. Photomask blanks comprising transmissive embedded phase shifter. *U.S. Patent No. 5,415,953*
54. Kalk FD, French RH, Alpay HU, Hughes G. 1994. Chromium-based attenuated embedded shifter preproduction. *SPIE* 2322:299–304
55. Smith JR, French RH, Duscher G, Bonnell DA. 2001. Consequence of composition/property variations at multiple length scales to macroscopic properties of CrOCN thin films. *J. Am. Ceram. Soc.* 84:2873–81
56. Carcia PF, French RH, Sharp K, Meth JS, Smith BW. 1996. Materials screening for attenuating embedded phase-shift photoblanks for DUV and 193 nm photolithography. *SPIE* 2884:255–63
57. Carcia PF, French RH, Reilly MH, Lemon MF, Jones DJ. 1997. Optical superlattices—a strategy for designing phase-shift masks for photolithography at 248 nm and 193 nm: application to AlN/CrN. *Appl. Phys. Lett.* 70:2371–73
58. Carcia PF, French RH, Reynolds G, Hughes G, Torardi CC, et al. 1999. Optical superlattices as phase-shift masks for microlithography. *SPIE* 3790:23–35
59. French RH, Sharp KG. 2000. Attenuating phase shift photomasks. *U.S. Patent No. 6,096,460*
60. Lai F. 2004. Optimized HT-AttPSM blanks using Al_2O_3/TiO_2 multilayer films for the 65 nm technology node. *J. Vac. Sci. Technol. B* 22:3097–101
61. Lai F, Juang CY, Ko F. 2007. The optical properties of monolayer amorphous Al_2O_3–TiO_2 composite films used as HT-APSM blanks for ArF immersion lithography. *Microelectron. Eng.* 84:716–20
62. Yang MK, French RH, Tokarsky EW. 2008. Optical properties of Teflon® AF amorphous fluoropolymers. *J. Micro/Nanolithogr. MEMS MOEMS* 7:033010
63. French RH, Wheland RC, Qiu W, Lemon MF, Zhang E, et al. 2003. Novel hydrofluorocarbon polymers for use as pellicles in 157 nm semiconductor photolithography. *J. Fluorine Chem.* 122:63–80
64. French RH, Wheland RC, Qiu W, Lemon MF, Zhang E, et al. 2002. 157 nm pellicles: polymer design for transparency and lifetime. *SPIE* 4691:1644–53
65. Lee K, Jockusch S, Turro NJ, French RH, Wheland RC, et al. 2004. 157 nm pellicles for photolithography: mechanistic investigation of the deep UV photolysis of fluorocarbons. *SPIE* 5377:1598–605
66. Urbach F. 1953. The long-wavelength edge of photographic sensitivity and of the electronic absorption of solids. *Phys. Rev.* 92:1324
67. Kunz RR, Switkes M, Sinta R, Curtin JE, French RH, et al. 2004. Transparent fluids for 157 nm immersion lithography. *J. Microlithogr. Microfabr. Microsyst.* 3:73–83
68. Burnett JH, Kaplan SG. 2004. Measurement of the refractive index and thermo-optic coefficient of water near 193 nm. *J. Microlithogr. Microfabr. Microsyst.* 3:68–72
69. Kaplan SG, Burnett JH. 2006. Optical properties of fluids for 248 and 193 nm immersion photolithography. *Appl. Opt.* 45:1721–24
70. López-Gejo J, Kunjappu JT, Turro NJ, Conley W. 2007. Amplification of the index of refraction of aqueous immersion fluids with crown ethers. *J. Microlithogr. Microfabr. Microsyst.* 6:013002
71. Zhou J, Fan Y, Bourov A, Cropanese F, Estroff A, Smith BW. 2005. Immersion fluids for high NA 193 nm lithography. *Proc. SPIE* 5754:630–37
72. Taylor JC, Costner EA, Goh S, Wojtczak W, Dewulf D, Willson CG. 2008. The effect of added salts on the optical properties of water for high index immersion lithography fluids. *J. Vac. Sci. Technol. B* 26:506–13
73. French RH, Qiu W, Yang MK, Wheland RC, Lemon MF, et al. 2006. Second generation fluids for 193 nm immersion lithography. *SPIE* ML6154–42
74. Santillan J, Otoguro A, Itani T, Fujii K, Kagayama A, et al. 2006. A study of 193-nm immersion lithography using novel high refractive index fluids. *Microelectron. Eng.* 83:651–54
75. Furukawa T, Kishida T, Miyamatsu T, Kawaguchi K, Yamada K, et al. 2007. High refractive index material design for ArF immersion lithography. *Proc. SPIE* 6519:65190B
76. Costner EA, Matsumoto K, Long BK, Taylor JC, Wojtczak W, Willson CG. 2008. New high-index fluids: exploiting anomalous dispersion for immersion lithography. *Proc. SPIE* 6923:69230B
77. Lopez-Gejo J, Kunjappu JT, Zhou J, Smith BW, Zimmerman P, et al. 2007. Polycycloalkanes as potential third-generation immersion fluids for photolithography at 193 nm. *Chem. Mater.* 19:3641–47

78. Zimmerman PA, Byers J, Piscani E, Rice B, Ober CK, et al. 2008. Development of an operational high refractive index resist for 193 nm immersion lithography. In *SPIE Proc.* Vol. 6923, *Adv. Resist Mater. Processing Technol. XXV*, ed. CL Henderson, Editors, p. 692306
79. Yang MK, Kaplan SG, French RH, Burnett JH. 2009. Index of refraction of high index lithographic immersion fluids and its variability. *J. Micro/Nanolithogr. MEMS MOEMS*. 8:023005
80. French RH, Liberman V, Tran HV, Feldman J, Adelman DJ, et al. 2007. High index immersion lithography with second generation immersion fluids to enable numerical apertures of 1.55 for cost effective 32 nm half pitches. *SPIE* ML6520-59:652010
81. Wei A, Abdo A, Nellis G, Engelstad RL, Chang J, et al. 2004. Modeling fluid thermomechanical response for immersion lithography scanning. *Microelectron. Eng.* 73–74:29–34
82. Burnett HB, Wei AC, El-Morsi MS, Shedd TA, Nellis GF, et al. 2006. Modeling and experimental investigation of bubble entrapment for flow over topography during immersion lithography. *J. Microlithogr. Microfabr. Microsyst.* 5:013008
83. Hinsberg W, Wallraff G, Larson C, Davis B, Deline V, et al. 2004. Liquid immersion lithography—evaluation of resist issues. *Proc. SPIE* 5376:21–33
84. Tran HV, French RH, Adelman DJ, Feldman J, Qiu W, et al. 2007. Evaluation of next generation fluids for ArF immersion lithography beyond water. *J. Photopolym. Sci. Technol.* 20:729–38
85. Nellis GF, El-Morsi MS, Peski CV, Grenville A. 2006. Contamination transport in immersion lithography. *J. Microlithogr. Microfabr. Microsyst.* 5:013007
86. Liberman VL, Rothschild M, Palmacci ST, Grenville A. 2007. Impact of photoacid generator leaching on optics photocontamination in 193-nm immersion lithography. *J. Microlithogr. Microfabr. Microsyst.* 6:013001
87. Taylor JC, LeSuer RJ, Chambers CR, Fan FF, Bard AJ, et al. 2005. Experimental techniques for detection of components extracted from model 193 nm immersion lithography photoresists. *Chem. Mater.* 17:4194–203
88. Wei Y, Stepanenko N, Laessig A, Voelkel L, Sebald M. 2006. Evaluation of 193-nm immersion resist without topcoat. *J. Microlithogr. Microfabr. Microsyst.* 5:0033002
89. Dammel RR, Pawlowski G, Romano A, Houlihan FM, Kim WK, et al. 2005. Resist component leaching in 193-nm immersion lithography. *Proc. SPIE* 5753:95–101
90. Houlihan F, Kim W, Sakamuri R, Hamilton K, Dimerli A, et al. 2005. Study of barrier coats for application in immersion 193-nm lithography. *Proc. SPIE* 5753:78–94
91. Gaugiran S, Feilleux R, Sourd C, Warrick S, Farys V, et al. 2007. Leaching mechanisms in immersion lithography with or without top coat. *Microelectron. Eng.* 84:1054–57
92. Maenhoudt M, Kocsis M, Stepanenko N, O'Brien S, Van Den Heuvel D, et al. 2006. Advances in immersion related defectivity on XT:1250i at IMEC. *J. Photopolym. Sci. Technol.* 19:585–91
93. Nakano K, Nagaoka S, Yoshida M, Iriuchijima Y, Fujiwara T, et al. 2008. Immersion defectivity study with volume production immersion lithography tool for 45 nm node and below. *Proc. SPIE* 6924:692418
94. Chibana T, Kobayashi M, Nakano H, Arakawa M, Matsuoka Y, et al. 2008. Immersion defect performance and particle control method for 45 nm mass production. *Proc. SPIE* 6924:69241B
95. Tran HV, Hendrickx E, French RH, Adelman DJ, Rogado NS, et al. 2008. High refractive index fluid evaluations at 193 nm: fluid lifetime and fluid/resist interaction studies. *J. Photopolym. Sci. Technol.* 21(No. 5):631–39
96. Allen RD, Brock PJ, Sundberg L, Larson CE, Wallraff GM, et al. 2005. Design of protective topcoats for immersion lithography. *J. Photopolym. Sci. Technol.* 18:615–19
97. Feiring AE, Feldman J, Schadt FL III, Leffew KW, Zumsteg FC, et al. 2003. Design of very transparent fluoropolymer resists for semiconductor manufacture at 157 nm. *J. Fluor. Chem.* 122:11–16
98. Toriumi M, Yamazaki T, Furukawa T, Irie S, Ishikawa S, Itani T. 2002. Fluoropolymer-based resists for a single-resist process of 157 nm lithography. *J. Vac. Sci. Technol. B* 20:2909–12
99. Feiring AE, Crawford MK, Farnham WB, French RH, Leffew KW, et al. 2006. Bis(fluoroalcohol) monomers and polymers: improved transparency fluoropolymer photoresists for semiconductor manufacture at 157 nm. *Macromolecules* 39:1443–48

100. Crawford MK, Farnham WB, Feiring AE, Feldman J, French RH, et al. 2003. Single layer fluoropolymer resists for 157 nm lithography. In *Advances in Resist Technology and Processing XX*, ed. TH Fedynyshyn, *Proc. SPIE* 5039, pp. 80–92
101. Feiring AE, Crawford MK, Farnham WB, Feldman J, French RH, et al. 2006. New amorphous fluoropolymers of tetrafluoroethylene with fluorinated and nonfluorinated tricyclononenes. Semiconductor photoresists for imaging at 157 and 193 nm. *Macromolecules* 39:3252–61
102. Sanders DP, Sundberg LK, Brock PJ, Ito H, Truong HD, et al. 2008. Self-segregating materials for immersion lithography. *Proc. SPIE* 6923(Pt. 1):692309
103. Kusumoto S, Shima M, Wang Y, Shimokawa T, Sato H, Hieda K. 2006. Advanced materials for 193 nm immersion lithography. *Polym. Adv. Technol.* 17:122–30
104. Sheehan MT, Farnham WB, Okazaki H, Sounik JR, Clark G. 2008. RAFT technology for the production of advanced photoresist polymers. In *Advances in Resist Materials and Processing Technology*, ed. CL Henderson, SPIE Proc. Vol. 6923, XXV, p. 69232E
105. Zimmerman PA, van Peski C, Rice B, Byers J, Turro NJ, et al. 2007. Status of high–index materials for generation-three 193 nm immersion lithography. *J. Photopolym. Sci. Technol.* 20:643–50
106. Zimmerman PA, Byers J, Piscani E, Rice B, Ober CK, et al. 2008. Development of an operational high refractive index resist for 193 nm immersion lithography. *Proc. SPIE* 6924:692306-1–10
107. Liu H, Blakey I, Conley WE, George GA, Hill DJT, Whittaker AK. 2008. Application of quantitative structure property relationship to the design of high refractive index 193i resist. *J. Microlithogr. Microfabr. Microsyst.* 7:023001
108. Matsumoto K, Costner EA, Nishimura I, Ueda M, Willson CG. 2008. High index resist for 193 nm immersion lithography. *Macromolecules* 41:5674–80
109. Hendrickx E, Postnikov S, Foubert P, Gronheid R, Kim B. 2007. Screening of second-generation high-index liquids. *Proc. SPIE* 6519(Pt. 1):65190A
110. Tran HV, Hendrickx E, Van Roey F, Vandenberghe G, French RH. 2009. Fluid-photoresist interactions and imaging in high index immersion lithography. *J. Micro/Nanolithogr. MEMS MOEMS.* Submitted
111. Bloomstein TM, Fedynyshyn TH, Pottebaum I, Marchant MF, Deneault SJ, Rothschild M. 2006. Immersion patterning down to 27 nm half pitch. *J. Vac. Sci. Technol. B* 24:2789–97
112. Sewell H, McCafferty D, Wagner C, Markoya L. 2005. Optical lithography for the 32 nm node. *J. Photopolym. Sci. Technol.* 18:579–86
113. Willson CG, Roman BJ. 2008. The future of lithography: SEMATECH litho forum 2008. *ACS Nano* 2:1323–28
114. Rice BJ. 2008. High-index immersion: materials challenges for optical extension. In *Semiconductor International Webcast on Preparing for High-Volume Immersion Lithography*. **http://www.semiconductor.net/webcastsDetail/2140141256.html?industryid=47484&industry=Technology+Webcasts**
115. Byers J, Lee S, Jen K, Zimmerman P, Turro NJ, Willson CG. 2007. Double exposure materials: simulation study of feasibility. *J. Photopolym. Sci. Technol.* 20:707–17
116. Lee S, Byers J, Jen K, Zimmerman P, Rice B, et al. 2008. An analysis of double exposure lithography options. *Proc. SPIE* 6924(Pt. 2):69242A
117. Yamaguchi M, Wallow T, Yamada Y, Kim R, Kye J, Levinson HJ. 2008. A study of photoresist pattern freezing for double imaging using 172nm VUV flood exposure. *J. Photopolym. Sci. Technol.* 21:697–704
118. Kim R, Levinson HJ. 2007. Application of contrast enhancement layer to 193 nm lithography. *J. Vac. Sci. Technol. B* 25:2466–70
119. Holmes SJ, Furukawa T, Hakey MC, Horak DV, Rabidoux PA, et al. 1999. Edge lithography as a means of extending the limits of optical and nonoptical lithographic resolution. *Proc. SPIE* 3678(Pt. 1):348–57
120. Maenhoudt M, Gronheid R, Stepanenko N, Matsuda T, Vangoidsenhoven D. 2008. Alternative process schemes for double patterning that eliminate the intermediate etch step. *Proc. SPIE* 6924(Pt. 1):69240P
121. Tarutani S, Tsubaki H, Kanna S. 2008. Development of materials and processes for double patterning toward 32 nm node ArF immersion lithography. *J. Photopolym. Sci. Technol.* 21:685–90
122. Ronse K. 2008. Water-based immersion lithography ramping further in 2008 and extendible for several generations through double patterning. In *Semiconductor International Webcast on Preparing for High-Volume Immersion Lithography*. **http://www.semiconductor.net/webcastsDetail/2140141256.html?industryid=47484&industry=Technology+Webcasts**

123. Abdallah DJ, Alemy E, Chakrapani S, Padmanaban M, Dammel RR. 2008. A novel resist freeze process for double imaging. *J. Photopolym. Sci. Technol.* 21:655–63
124. Chen KR, Huang W, Li W, Varanasi PR. 2008. Resist freezing process for double exposure lithography. *Proc. SPIE* 6923(Pt. 1):69230G
125. Anno Y, Kakizawa T, Hori M, Soyano A, Fujiwara K, et al. 2008. Double patterning materials for sub40 nm application. *J. Photopolym. Sci. Technol.* 21:691–96
126. Bencher C. 2007. SADP: The Best Option for < 32 nm NAND flash. *Nanochip Technol. J.* 2:8–13
127. Jung W, Kim S, Kim C, Sim G, Jeon S, et al. 2007. Patterning with amorphous carbon spacer for expanding the resolution limit of current lithography tool. *Proc. SPIE* 6520(Pt. 1):65201C
128. Dusa M, Quaedackers J, Larsen OFA, Meessen J, van der Heijden E, et al. 2007. Pitch doubling through dual-patterning lithography challenges in integration and litho budgets. *Proc. SPIE* 6520:65200G
129. Raub AK, Li D, Frauenglass A, Brueck SRJ. 2007. Fabrication of 22 nm half-pitch silicon lines by single-exposure self-aligned spatial-frequency doubling. *J. Vac. Sci. Technol. B* 25:2224–27
130. Schellenberg FM, ed. 2004. *Selected Papers on Resolution Enhancement Techniques in Optical Lithography*, SPIE Milestone Ser., Vol. MS 178. Bellingham, WA: SPIE Press

Annual Review of
Materials Research

Volume 39, 2009

Contents

Materials Advances for Next-Generation Microelectronics

Current Interest

Index

Errata

An online log of corrections to *Annual Review of Materials Research* articles may be found at http://matsci.annualreviews.org/errata.shtml